THE JOURNAL OF PHYSICAL CHEMISTRY A
A JOURNAL OF THE AMERICAN CHEMICAL SOCIETY

pubs.acs.org/JPCA Article

Gradients of Ground and Excited States for CC2 and ADC(2) in Polarizable Continuum and Atomistic Embeddings within a Generalized PTED Coupling Scheme

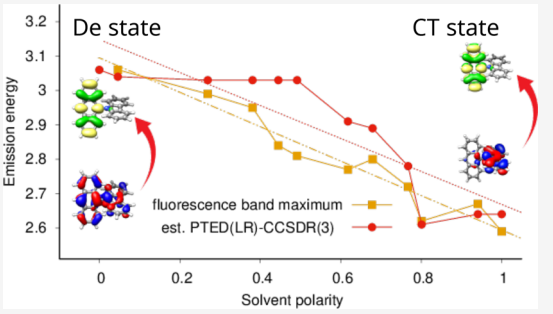
Published as part of The Journal of Physical Chemistry A special issue "Forty Years of Response Function Theory".

Christof Hättig* and Ansgar Pausch*

Cite This: https://doi.org/10.1021/acs.jpca.5c02873 Read Online

ACCESS | Metrics & More | Article Recommendations

ABSTRACT: We present a state-specific implementation of ground and excitation energies and analytic gradients thereof for the approximate coupled-cluster singles and doubles model CC2 in polarizable environments that is suitable for the description of long-living charge-transfer excited states. It employs a reaction field potential equilibrated self-consistently with the target state density and includes linear response contributions to account for the excitonic coupling to the optical polarizability of the environment. The implementation is available in combination with the conductor-like screening model COSMO as a polarizable continuum model and an atomistic polarizable embedding in point multipoles and polarizabilities. For COSMO smooth potential energy surfaces and convergence of structure optimizations are obtained with a Gaussian charge model. For the algebraic-diagrammatic construction through second order, ADC(2), with COSMO, it is identical to an earlier implementation [Lunkenheimer, B. and Köhn, A. *J. Chem. Theory Comput.* **2013**, *9*, 977−994] but extends the latter to analytic gradients. Example applications are presented for structures, dipole moments, and emission energies of the charge-transfer and locally excited states of 4-(*N*,*N*-dimethylamino)benzonitrile and *N*-(9-anthryl)carbazole in different solvents. The results demonstrate that not only solvent shifts but also physically correct structures are obtained for strongly polar states in polarizable environments.



INTRODUCTION

Polar and polarizable environments often have large effects on the spectra and photophysical properties of molecules.[1,2] In particular, if the studied molecule exhibits excited states with significant charge-transfer contributions, the polarity and polarizability of its environment have a large influence on the relative energies of electronic states and, by modulating configuration mixing, on the character of electronic states.[3,4] The latter also influences potential energy surfaces and the molecular structure, i.e., bond lengths, bond angles, and torsion angles.[5,6] Because of the steep cost scaling of accurate electronic structure calculations for electronically excited states with system size, environment effects are often included by coupling such calculations on the chromophore via self-consistent reaction field (SCRF) theory to simplified descriptions of the environment.[7] This leads, for the electronic structure of the chromophore, to nonlinear Schrödinger equations with an environment (reaction field) potential that depends on the chromophore's charge distribution in a reference state with which the polarizable environment is equilibrated.

Since the seminal work of Olsen and Jørgensen,[8] response function theory has become one of the most widely used theoretical frameworks for the calculation of excitation energies and excited-state potential energy surfaces. Its success stems from its applicability to a wide range of wave function parametrizations including single- and multiconfigurational self-consistent field[8] and coupled-cluster[9] wave functions. In vacuum, it gives, for linear wave function parametrizations or in the full configuration interaction limit, equivalent results as state-specific wave function optimizations. This equivalence is, however, lost if it is used in the SCRF framework. Response function theory and state-specific approaches account then for different contributions to the interaction with the environment and give deviating results, which causes complications (vide

Received: April 26, 2025
Revised: May 31, 2025
Accepted: June 5, 2025

Downloaded via RUHR UNIVERSITAT BOCHUM on June 30, 2025 at 06:58:23 (UTC).
See https://pubs.acs.org/sharingguidelines for options on how to legitimately share published articles.

ACS Publications © XXXX American Chemical Society

infra). For implicit solvent models such as the conductor-like screening model (COSMO),[10,11] which approximate a thermally averaged reaction field potential, further complications arise from the different time scales for equilibration of the electronic and nuclear (orientational) polarizability of the environment.

This complexity led, in combination with approximate electronic structure methods, to a plethora of different reaction field schemes for coupling electronic structure calculations for electronic ground and excited states to polarizable environments, which differ vastly in the physical situations they are suited for, as well in computational costs and complexity of the implementations. Analytic ground- and excited-state gradients—essential for studying relaxation processes, fluorescence emission, and other excited-state properties—are available for only very few reaction field coupling schemes. For time-dependent density functional theory, analytic excited-state gradients including solvent effects have only been reported for the linear response (LR) coupling scheme[12] and the vertical excitation model with the unrelaxed difference density[12] (VEM-UD). Similarly, implementations of analytic excited-state gradients have been reported for the polarizable continuum model[13] (PCM) combined with symmetry-adapted cluster configuration interaction (SAC-CI) with the state-specific perturbation through the energy and density (PTED) coupling scheme[14] and with coupled-cluster singles and doubles (CCSD) for the LR and the PTED coupling schemes.[15−17] For the algebraic-diagrammatic construction through second order, ADC(2), analytic excited-state gradients in polarizable continuum or atomistically modeled environments are yet only available for an LR approach.[18,19] For the related approximate CCSD model,[20] CC2 analytic excited-state gradients in polarizable environments have not yet been reported.

While the LR coupling scheme includes the excitonic coupling of the solute's transition density to the polarizability of the environment, the state-specific VEM-UD and PTED schemes account for the changes of the environment's charge distribution due to the redistribution of the solute's charge density in the excited state.[21] The former contribution is important for bright states with large transition densities, and the latter is important for charge-transfer (CT) states, where the density change upon excitation is larger. For a balanced treatment of transitions with different characters, however, both contributions must be included.

In the current work, we report analytic excited-state gradients for the wave function-based second-order models ADC(2) and CC2 coupled to polarizable environments through a generalized PTED scheme, which was first proposed in ref 21 for excitation energies with COSMO-ADC(2). This coupling scheme, which is in the following denoted as PTED(LR), includes the state-specific (SS) contributions due to the charge redistribution in the excited state as well as the LR contribution.[21] An implementation of the excited-state gradients is presented for COSMO[10] and an atomistic polarizable embedding[22] (PE). The performance of the PTED(LR) scheme for excited-state structures and emission energies in solution is demonstrated for locally excited (LE) and CT states in 4-(*N*,*N*-dimethylamino)benzonitrile (DMABN) and the delocalized S_1 state in N-(9-anthryl)carbazole (C9A).

METHODS

Conductor-like Screening Model. Like several other polarizable continuum models, COSMO belongs to the apparent surface methods that represent the polarization induced by a solute in the surrounding solvent by charges positioned on the surface of a cavity surrounding the solute. The solvent is approximated as a homogeneous isotropic dielectric continuum. In COSMO, the surface charges are calculated as[10]

$$Q_\mu(\mathbf{D}) = -f(\epsilon) \sum_\nu [\mathcal{A}^{-1}]_{\mu\nu} V_\nu(\mathbf{D}) \tag{1}$$

where $V_\mu(\mathbf{D})$ are the values of the Coulomb potentials for the individual surface segments μ due to the solute's charge density $\mathbf{D}$ and $\mathcal{A}$ is the response kernel for COSMO. $f(\epsilon)$ is a scaling factor depending on the dielectric constant ϵ:

$$f(\epsilon) = \frac{\epsilon - 1}{\epsilon + 0.5} \tag{2}$$

The precise expressions for V_μ and $\mathcal{A}$ depend on the actual implementation. We employ for the current work the COSMO implementation with a Gaussian charge model[23,24] (COSMO-GCM) of ref 25 and refer to the latter work for detailed equations. The reaction field operator describing the potential that is experienced by the solute due to induced surface charges for COSMO is, in second quantization, given by

$$\hat{G}(\mathbf{D}) = \sum_\mu Q_\mu(\mathbf{D}) \sum_{pq} V_{pq,\mu} E_{pq} \tag{3}$$

where E_{pq} are the second quantization singlet operators[26] for the molecular orbitals (MOs) p and q, and

$$V_{pq,\mu} = \frac{\partial V_\mu(\mathbf{D})}{\partial D_{pq}} \tag{4}$$

Below, we will in addition use the operators

$$\hat{V}_\mu = \sum_{pq} V_{pq,\mu} E_{pq} \tag{5}$$

for the potentials at the individual surface segments. For electronic excitations, the reaction field can also couple to the transition density of the excitation if the environment has a nonzero optical polarizability. For this so-called linear response contribution,[18,21] the scaling factor is determined from the square of the refractive index n. Charges and reaction field potentials calculated with only the fast, optical component of the reaction field will in the following be indicated with an upper index *fast*:

$$Q_\mu^{\text{fast}}(\mathbf{D}) = -f(n^2) \sum_\nu [\mathcal{A}^{-1}]_{\mu\nu} V_\nu(\mathbf{D}) \tag{6}$$

$$\hat{G}^{\text{fast}}(\mathbf{D}) = \sum_\mu Q_\mu^{\text{fast}}(\mathbf{D}) \hat{V}_\mu \tag{7}$$

Polarizable Embedding. The polarizable embedding[27] (PE) is a hybrid quantum mechanical and molecular mechanics (QM/MM) method where the electrostatic part of the environment is represented by static charges and multipole moments, Q_u^{es}, and distributed multipole polarizabilities, α_{uv}. For simplicity, we use here and in the following u and v as compound indices for site, rank, and component of the multipoles and polarizabilities. The polarizabilities lead to induced moments

$$Q_v^{\text{ind}}(\mathbf{D}) = -\sum_u R_{vu}(V_u(\mathbf{D}) + V_u^{\text{es}}) \tag{8}$$

https://doi.org/10.1021/acs.jpca.5c02873
J. Phys. Chem. A XXXX, XXX, XXX−XXX

where $\mathbf{R}$ is a classical response matrix built from the polarizabilities and multipole interaction tensors.[27] $V_u(\mathbf{D})$ and V_u^{es} are the electrostatic potentials or potential derivatives for site, rank, and component u due to, respectively, the solute's charge distribution and the static multipole moments of the environment.[19,28] In analogy to COSMO, we introduce the operators

$$\hat{V}_u = \sum_{pq} V_{pq,u} E_{pq} \tag{9}$$

for the interaction of the electrons with a given multipole moment Q_u.

QM/MM calculations modeling the environments by point charges and multipoles often suffer, for electronic excitation energies, from large errors due to electron spill-out if large basis sets are used.[29] To avoid this, we use for the current work an extension[29] denoted as PE(ECP), which includes at the MM sites all-electron effective core potentials (ECPs) to account for the Pauli repulsion. The total reaction field operator acting on the solute's electrons is then given by

$$\hat{G}(\mathbf{D}) = \hat{G}^{\mathrm{pol}}(\mathbf{D}) + \hat{G}^{\mathrm{es}} + \hat{V}^{\mathrm{ECP}} \tag{10}$$

$$\hat{G}^{\mathrm{pol}}(\mathbf{D}) = \sum_u Q_u^{\mathrm{ind}}(\mathbf{D}) \hat{V}_u \tag{11}$$

$$\hat{G}^{es} = \sum_u Q_u^{es} \hat{V}_u \tag{12}$$

To the LR of the reaction field to changes in the electron density, only the response of the induced moments, Q_u^{ind}, contributes. In contrast to the case of COSMO, the PE does not implicitly account for polarization contributions from relaxations of the nuclear positions in the environment. The polarizabilities α_{uv} describe only the fast electronic polarizability of the latter. A distinction between slow (nuclear) and fast (electronic) polarization of the environment—as done in COSMO—is not used in PE models.

In addition to the electrostatic interactions and the ECPs that act on the electrons of the QM system, TURBOMOLE's PE implementation[19] includes in the energy expression Lennard-Jones 6−12 potentials between the QM system and the environment

$$E^{\mathrm{LJ}} = \sum_s^{\mathrm{env}} \sum_m^{\mathrm{QM}} \epsilon^{sm} \left[\left(\frac{r_{sm}}{|\mathbf{R}_m - \mathbf{R}_s|} \right)^{12} - 2 \left(\frac{r_{sm}}{|\mathbf{R}_m - \mathbf{R}_s|} \right)^{6} \right] \tag{13}$$

to obtain physically correct potential energy surfaces. In the above equation, ϵ^{sm} and r_{sm} are the parameters for, respectively, the well depth and optimal distance for atoms s and m.

Orbital-Relaxed One-Electron Densities for CC2 and ADC(2). To introduce the basic concepts and notation for the calculation of orbital-relaxed densities for correlated wave function methods, we start with an isolated quantum system. In the standard coupled-cluster methods, the energy of an isolated quantum system is determined as

$$E_{\mathrm{CC}} = \langle \mathrm{HF} | \hat{H} \exp(\hat{T}) | \mathrm{HF} \rangle \tag{14}$$

where $|\mathrm{HF}\rangle$ is the Hartree−Fock reference determinant and $\hat{T}$ is the cluster operator. For simplicity, we assume for the following a closed-shell reference state and use a spin-free formulation for the contributions to the cluster operator:

$$\hat{T} = \hat{T}_1 + \hat{T}_2 + \cdots \tag{15}$$

$$\hat{T}_1 = \sum_{ai} t_{ai} E_{ai} \tag{16}$$

$$\hat{T}_2 = \sum_{ai \geq bj} t_{aibj} E_{ai} E_{bj} \tag{17}$$

Here and in the following, we use the convention that $a, b, c, \cdots$ denote virtual, $i, j, k, \cdots$ denote occupied, and $p, q, r, \cdots$ denote general MOs. For the approximate coupled-cluster singles and doubles model CC2, the singles and doubles amplitudes are determined by the following equations:[20]

$$0 = \langle \mu_1 | \widehat{\widehat{H}} + [\widehat{\widehat{W}}, \hat{T}_2] | \mathrm{HF} \rangle \tag{18}$$

$$0 = \langle \mu_2 | \widehat{\widehat{W}} + [\hat{F}, \hat{T}_2] | \mathrm{HF} \rangle \tag{19}$$

Above, $\hat{F}$ and $\hat{W} = \hat{H} - \hat{F}$ are, respectively, the Fock operator and the fluctuation potential, and we introduced the short-hand notation $\hat{\bar{O}} = \exp(-\hat{T}_1)\hat{O}\exp(\hat{T}_1)$ for operators that have been similarity-transformed with $\exp(\hat{T}_1)$. The singly and doubly excited subsets of the projection manifold are denoted by $\langle \mu_1|$ and $\langle \mu_2|$, respectively. We employ the biorthonormal projection manifold[26] with $\langle {}^{a}_{i}| = \frac{1}{2}\langle \mathrm{HF}|E_{ia}$ and $\langle {}^{ab}_{ij}| = \frac{1}{3}\langle \mathrm{HF}|E_{jb}E_{ia} + \frac{1}{6}\langle \mathrm{HF}|E_{ja}E_{ib}$.

For the calculation of energy derivatives, it is convenient to parametrize the Hartree−Fock wave function as

$$|\mathrm{HF}\rangle = \exp\Big(\sum_{\mu_0} \kappa_{\mu_0} (E_{\mu_0} - E_{\mu_0}^{\dagger})\Big) |\mathrm{HF}_0\rangle \tag{20}$$

where $|\mathrm{HF}_0\rangle$ is the reference determinant for the unperturbed system, and to combine eqs 14, 18, and 19 together with the Brillouin condition $\langle \mathrm{HF}|[\hat{H}, \hat{a}_c^{\dagger}\hat{a}_k]|\mathrm{HF}\rangle = 0$ to a variational Lagrange function:[30]

$$\begin{aligned} L_{\mathrm{CC2}}(\bar{t}, t, \bar{\kappa}, \kappa) = {} & \left\langle \mathrm{HF} \middle| \widehat{\widehat{H}} + \left[\widehat{\widehat{W}}, \hat{T}_2 \right] \middle| \mathrm{HF} \right\rangle + \left\langle \mathrm{HF} \middle| \left[\widehat{\widehat{H}}, \hat{\bar{\kappa}} \right] \middle| \mathrm{HF} \right\rangle \\ & + \left\langle \bar{t}_1 \middle| \widehat{\widehat{H}} + \left[\widehat{\widehat{W}}, \hat{T}_2 \right] \middle| \mathrm{HF} \right\rangle + \left\langle \bar{t}_2 \middle| \widehat{\widehat{W}} + \left[\hat{F}, \hat{T}_2 \right] \middle| \mathrm{HF} \right\rangle \end{aligned} \tag{21}$$

The auxiliary singly and doubly excited bra states are defined as $\langle \bar{t}_i| = \sum_{\mu_i} \bar{t}_{\mu_i} \langle \mu_i|$, where the indices μ_1 and μ_2 run over, respectively, single and double excitations. $\hat{\bar{\kappa}} = \sum_{\mu_0} \bar{\kappa}_{\mu_0} (E_{\mu_0} - E_{\mu_0}{}^{\dagger})$, and the index μ_0 runs over the set of orbital pairs $p > q$ for which the Fock matrix elements are required to vanish.[30] Once the cluster amplitudes t_{μ_i} and Lagrange multipliers $\bar{t}_{\mu_i}$ and $\bar{\kappa}_{\mu_0}$ have been determined from the condition that L_{CC2} is stationary in all its variables, orbital-relaxed first derivatives of the CC2 energy can be calculated similarly as for variational methods by contracting differentiated integrals with unperturbed densities. For example, one-electron first-order properties can be calculated as

$$\langle O \rangle = \sum_{pq} O_{pq} D_{pq}^{\mathrm{CC2,eff}} \tag{22}$$

with the effective or orbital-relaxed one-electron CC2 density:

$$\begin{aligned} D_{pq}^{\mathrm{CC2,eff}} = {} & \left\langle \mathrm{HF} \middle| e^{-\hat{T}_1} E_{pq} e^{\hat{T}_1} + \left[E_{pq}, \hat{\bar{\kappa}} \right] \middle| \mathrm{HF} \right\rangle \\ & + \left\langle \bar{t}_1 \middle| e^{-\hat{T}_1} \left(\left[E_{pq}, \hat{T}_2 \right] + E_{pq} \right) e^{\hat{T}_1} \middle| \mathrm{HF} \right\rangle + \left\langle \bar{t}_2 \middle| \left[E_{pq}, \hat{T}_2 \right] \middle| \mathrm{HF} \right\rangle \end{aligned} \tag{23}$$

https://doi.org/10.1021/acs.jpca.5c02873
J. Phys. Chem. A XXXX, XXX, XXX−XXX

The latter density is of particular interest when the interaction of the QM system with a polarizable environment is treated within the PTED coupling scheme, where the charge density of the QM system and the reaction field potential of the environment are determined self-consistently at the level of the correlated post-Hartree−Fock method.

Excitation energies are, in coupled-cluster response theory, determined as eigenvalues of the Jacobian

$$A_{\mu\nu}^{\mathrm{CC2}} = \frac{\partial^2 L_{\mathrm{CC2}}}{\partial \overline{t}_\mu \partial t_\nu} \tag{24}$$

or, in second quantization

$$\mathbf{A}^{\mathrm{CC2}} = \left(\begin{array}{c|c} \langle {}^{a}_{i}|[\hat{\tilde{H}} + [\hat{H}, \hat{T}_2], E_{ck}]|\mathrm{HF}\rangle & \langle {}^{a}_{i}|[\hat{\tilde{H}}, E_{ck}E_{dl}]|\mathrm{HF}\rangle \\ \hline \langle {}^{ab}_{ij}|[\hat{\tilde{H}}, E_{ck}]|\mathrm{HF}\rangle & \langle {}^{ab}_{ij}|[\hat{F}, E_{ck}E_{dl}]|\mathrm{HF}\rangle \end{array} \right) . \tag{25}$$

The Lagrangian for the total energy of an excited state f can be expressed as the sum of the ground-state Lagrange function plus a contribution for the excitation energy:[31,32]

$$\begin{aligned} L^f_{\mathrm{CC2}}(\overline{t}^f,\ t,\ \overline{\kappa}^f,\ \kappa,\ \overline{E}^f,\ E^f,\ \overline{\omega}^f) &= L_{\mathrm{CC2}}(\overline{t}^f,\ t,\ \overline{\kappa}^f,\ \kappa) + \sum_{i,j=1}^{2} \sum_{\mu_i\nu_j} \overline{E}^f_{\mu_i} A^{\mathrm{CC2}}_{\mu_i\nu_j} E^f_{\nu_j} \\ &\quad + \overline{\omega}^f \left(1 - \sum_{i=1}^{2} \sum_{\mu_j} \overline{E}^f_{\mu_i} E^f_{\mu_j}\right) \end{aligned} \tag{26}$$

In the last equation, an upper index f is used for the Lagrange multipliers $\overline{t}^f$ and $\overline{\kappa}^f$ to indicate their dependence on the excited state, and $\overline{E}^f$ and E^f are, respectively, the left and right eigenvectors for the excitation to state f. The second term accounts for the excitation energy, and the last term constrains the eigenvectors to be biorthonormalized. Similarly, the expression for the orbital-relaxed one-electron density for an excited state f consists of contributions from the excitation as well as ground-state-like contributions:

$$\begin{aligned} D^{\mathrm{CC2},f,\mathrm{eff}}_{pq} &= \left\langle \mathrm{HF} \middle| e^{-\hat{T}_1} E_{pq} e^{\hat{T}_1} + \left[E_{pq},\ \hat{\overline{\kappa}}^f\right] \middle| \mathrm{HF} \right\rangle \\ &\quad + \left\langle \overline{t}^f_1 \middle| e^{-\hat{T^{\wedge}}_1} \left(\left[E_{pq},\ \hat{T}_2\right] + E_{pq} \right) e^{\hat{T}_1} \middle| \mathrm{HF} \right\rangle \\ &\quad + \left\langle \overline{t}^f_2 \middle| \left[E_{pq},\ \overline{T}_2\right] \middle| \mathrm{HF} \right\rangle \\ &\quad + \left\langle \overline{E}^f_1 \middle| e^{-\hat{T}_1} \left[E_{pq},\ \hat{E}^f_1 + \hat{E}^f_2\right] e^{\hat{T}_1} \middle| \mathrm{HF} \right\rangle \\ &\quad + \left\langle \overline{E}^f_2 \middle| \left[E_{pq},\ \hat{E}^f_2\right] \middle| \mathrm{HF} \right\rangle \end{aligned} \tag{27}$$

Above, we introduced the auxiliary operators $\hat{E}^f_1 = \sum_{ai} E^f_{ai} E_{ai}$ and $\hat{E}^f_2 = \sum_{ai\geq bj} E^f_{aibj} E_{ai} E_{bj}$ and bra states $\langle \overline{E}_i| = \sum_{\mu_i} \overline{E}_{\mu_i} \langle \mu_i|$.

In the algebraic-diagrammatic construction,[33] the excitation energies are determined as eigenvalues of a secular matrix, which is derived from a perturbation expansion of the polarization propagator. For ADC(2), the expansion is truncated in second order[33,34] and, similar to second-order Møller−Plesset perturbation theory for the ground-state energy, it needs the first-order ground-state doubles amplitudes, $t_{\mu_2}{}^{(1)}$. If the Hartree−Fock reference determinant fulfills the Brillouin condition, then no ground-state singles amplitudes appear in the expressions for ADC(2) and MP2. Because of the close relation between ADC(2) and MP2, the excitation energies obtained with ADC(2) are usually combined with MP2 ground-state energies to define total energies, potential energy surfaces, and properties of the excited states.[35] The Lagrange function for the ADC(2) excited-state total energies can then technically be generated from the expression for L^f_{CC2} by skipping the contributions from the ground-state singles amplitudes t_{μ_1} and multipliers $\overline{t}_{\mu_1}{}^f$ and taking only the Hermitian part of the singles/singles block[35] of $\mathbf{A}$:

$$\begin{aligned} L^f_{\mathrm{ADC(2)}}(\overline{t}^f,\ t,\ \overline{\kappa}^f,\ \kappa,\ \overline{E}^f, E^f, \overline{\omega}^f) &= L_{\mathrm{MP2}}(\overline{t}^f,\ t,\ \overline{\kappa}^f,\ \kappa) + \sum_{i,j=1}^{2} \sum_{\mu_i\nu_j} \overline{E}^f_{\mu_i} A^{\mathrm{ADC(2)}}_{\mu_i\nu_j} E^f_{\nu_j} \\ &\quad + \overline{\omega}^f \left(1 - \sum_{i=1}^{2} \sum_{\mu_i} \overline{E}^f_{\mu_i} E^f_{\mu_i}\right) \end{aligned} \tag{28}$$

with

$$\begin{aligned} L_{\mathrm{MP2}}(\overline{t},\ t,\ \overline{\kappa},\ \kappa) &= \langle \mathrm{HF}|\widehat{H} + [\widehat{W},\ \widehat{T}_2]|\mathrm{HF}\rangle + \langle \mathrm{HF}|[\widehat{H},\ \widehat{\kappa}]|\mathrm{HF}\rangle \\ &\quad + \langle \overline{t}_2|\widehat{W} + [\widehat{F},\ \widehat{T}_2]|\mathrm{HF}\rangle \end{aligned} \tag{29}$$

For the ADC(2) secular matrix, we use the second quantization expression in the biorthonormal spin-free excitation and projection manifold:[26]

$$\mathbf{A}^{\mathrm{ADC(2)}} = \left(\begin{array}{c|c} \hat{P}^{ac}_{ik} \langle {}^{a}_{i}|\tfrac{1}{2}[\hat{H}, E_{ck}] + [[\hat{H}, \hat{T}_2], E_{ck}]|\mathrm{HF}\rangle & \langle {}^{a}_{i}|[\hat{H}, E_{ck}E_{dl}]|\mathrm{HF}\rangle \\ \hline \langle {}^{ab}_{ij}|[\hat{H}, E_{ck}]|\mathrm{HF}\rangle & \langle {}^{ab}_{ij}|[\hat{F}, E_{ck}E_{dl}]|\mathrm{HF}\rangle \end{array} \right) . \tag{30}$$

The operator $\hat{P}^{ab}_{ij}$ symmetrizes with respect to the interchanges of the index pairs ai and bj.

The expressions for the respective orbital-relaxed one-electron densities are

$$\begin{aligned} D^{\mathrm{MP2,eff}}_{pq} &= \left\langle \mathrm{HF} \middle| E_{pq} + \left[E_{pq},\ \hat{\overline{\kappa}}\right] \middle| \mathrm{HF} \right\rangle \\ &\quad + \left\langle \overline{t}_2 \middle| \left[E_{pq},\ \hat{T}_2\right] \middle| \mathrm{HF} \right\rangle \end{aligned} \tag{31}$$

and

$$\begin{aligned} D^{\mathrm{ADC(2)},f,\mathrm{eff}}_{pq} &= \left\langle \mathrm{HF}|E_{pq} + [E_{pq},\ \hat{\overline{\kappa}}^f]|\mathrm{HF}\right\rangle \\ &\quad + \left\langle \overline{t}^f_2|[E_{pq},\ \hat{T}_2]|\mathrm{HF}\right\rangle \\ &\quad + \left\langle \overline{E}^f_1|[E_{pq},\ \hat{E}^f_1 + \hat{E}^f_2]|\mathrm{HF}\right\rangle \\ &\quad + \left\langle \overline{E}^f_2|[E_{pq},\ \hat{E}^f_2]|\mathrm{HF}\right\rangle \end{aligned} \tag{32}$$

PTED-ADC(2) and PTED-CC2. Within the PTED coupling scheme, the potential of the polarized environment (the "reaction field") and the polarized charge distribution of the embedded quantum system (the "solute") are equilibrated until self-consistency is reached for a correlated and/or electronically excited post-HF wave function. The SCRF problem is solved in a loop over Hartree−Fock and post-HF calculations:

1. solution of the Hartree−Fock equations for a fixed reaction field potential $\hat{G}(\mathbf{D})$;
2. solution of the post-HF problem, i.e., for CC2, the cluster and Lagrange multiplier equations and, for excited states, the eigenvalue equations;

https://doi.org/10.1021/acs.jpca.5c02873
J. Phys. Chem. A XXXX, XXX, XXX−XXX

3. calculation of the one-electron density matrix **D** for the correlated and/or electronically excited state and the reaction field potential $\hat{G}(\mathbf{D})$; and

4. convergence check; if not yet converged, continue with step 1.

The PTED scheme was initially proposed for Møller−Plesset perturbation theory in connection with PCM[36] and has been implemented using the unrelaxed and the relaxed correlated density for different descriptions of the environment.[37] It has also been combined with other electronic structure methods such as, e.g., PCM-CCSD for ground- and excited-state energies.[15,16,38,39]

Lunkenheimer and Köhn[21] implemented the PTED coupling scheme for the resolution-of-the-identity (RI) variants of ADC(2) and MP2 in combination with COSMO for the calculation of electronic excitation energies and spectra in solution. Their implementation calculates the reaction field potential $\hat{G}$ from the orbital-relaxed one-electron densities of either the ground state described by MP2 or an electronically excited state at the ADC(2) level. The motivation for this choice has been that the orbital-relaxed density includes contributions from the orbital response and allows consistency through the second-order perturbation theory (for the density) without the need to calculate second-order amplitudes.[21] The latter would increase the cost scaling from $O(N^5)$ to $O(N^6)$. An important second advantage of this choice, not mentioned in ref 21 but equally important for the current work, is that in the SCRF iterations a Lagrange functional is made stationary, which differs from the vacuum case only in the interaction of the cavity surface charges with the potential on the surface. For PTED-COSMO-MP2 with $\hat{G}$ calculated from the orbital-relaxed density, the Lagrangian is

$$L_{\text{PTED-COSMO-MP2}}\left(\bar{t},\ t,\ \bar{\kappa},\ \kappa\right) = L_{\text{MP2}}\left(\bar{t},\ t,\ \bar{\kappa},\ \kappa\right) + \frac{1}{2}\sum_{\nu} Q_{\nu}\left(\mathbf{D}^{\text{MP2,eff}}\right)\cdot V_{\nu}\left(\mathbf{D}^{\text{MP2,eff}}\right) \tag{33}$$

and similarly for a pure SS PTED-COSMO-ADC(2) without LR contributions:

$$L^{f}_{\text{PTED-COSMO-ADC(2)}}(\bar{t}^{f},\ t,\ \bar{\kappa}^{f},\ \kappa,\ \bar{E}^{f},\ E^{f},\ \bar{\omega}^{f}) = L^{f}_{\text{ADC(2)}}(\bar{t}^{f},\ t,\ \bar{\kappa}^{f},\ \kappa,\ \bar{E}^{f},\ E^{f},\ \bar{\omega}^{f}) + \frac{1}{2}\sum_{\nu} Q_{\nu}(\mathbf{D}^{\text{ADC(2)},f,\text{eff}})\cdot V_{\nu}(\mathbf{D}^{\text{ADC(2)},f,\text{eff}}) \tag{34}$$

No equations for additional Lagrange multipliers, which would not be present in the vacuum case, need to be solved, and the expressions for the densities, eqs 31 and 32, remain unchanged. The simplicity of the Lagrange functions also makes the implementation of nuclear gradients a straightforward task (vide infra).

As mentioned above, for electronically excited states, the PTED coupling scheme fully accounts for charge redistributions in the equilibrated excited state relative to the ground state. This is especially important for CT states. The secular matrix obtained for this variant of PTED-COSMO-ADC(2) is

$$\mathbf{A}^{\text{PTED-ADC(2)}} = \mathbf{A}^{\text{ADC(2)}} + \begin{pmatrix} \langle {}^{a}_{i}|[\hat{G}, E_{ck}]|\text{HF}\rangle & 0 \\ 0 & \langle {}^{ab}_{ij}|[\hat{G}, E_{ck}E_{dl}]|\text{HF}\rangle \end{pmatrix} . \tag{35}$$

The additional contributions are easily included by replacing the vacuum-like Fock operator $\hat{F}$ by $\hat{F}^{\text{emb}} = \hat{F} + \hat{G}$, where $\hat{G}$ is calculated from the $\mathbf{D}^{\text{ADC(2)},f,\text{eff}}$ of the equilibrated state f.

Without further correction, the PTED scheme does, however, not include the so-called LR terms,[21,40,41] which account for the effect of electronic excitation energy transfer or excitonic coupling to the surrounding solvent. The latter red-shift excitation energies depending on the magnitude of the transition density by up to a few 0.1 eV. Therefore, Lunkenheimer and Köhn proposed to include the response terms for excited states in the PTED coupling scheme in addition to the interaction of the environment with the permanent charge distribution of the solute.[21] The LR contributions up to second order enter only in the singles/singles block of the secular matrix. For COSMO, they are

$$\mathbf{A}^{\text{ADC(2),rsp}}_{ai,ck} = \frac{1}{2}\hat{P}^{ac}_{ik}\sum_{\lambda}\langle {}^{a}_{i}|\hat{V}_{\lambda} + [\hat{V}_{\lambda},\ \hat{T}_2]|\text{HF}\rangle \times \langle \text{HF}|[\hat{Q}^{\text{fast}}_{\lambda},\ E_{ck}]|\text{HF}\rangle \tag{36}$$

Because of the advantages of $\hat{G}$ calculated from the orbital-relaxed density, in particular, the simplicity of the Lagrange function, we follow the same approach for the implementation of the PTED coupling scheme for ground and electronically excited states with CC2. For the electronic ground state with COSMO as the solvation model, the Lagrange function becomes

$$L_{\text{PTED-COSMO-CC2}}(\bar{t},\ t,\ \bar{\kappa},\ \kappa) = L_{\text{CC2}}(\bar{t},\ t,\ \bar{\kappa},\ \kappa) + \frac{1}{2}\sum_{\mu} Q_{\mu}(\mathbf{D}^{\text{CC2,eff}})\cdot V_{\mu}(\mathbf{D}^{\text{CC2,eff}}) \tag{37}$$

and similarly for excited states if no LR contributions are included:

$$L^{f}_{\text{PTED-COSMO-CC2}}(\bar{t},\ t,\ \bar{\kappa},\ \kappa,\ \bar{E}^{f},\ E^{f},\ \bar{\omega}^{f}) = L^{f}_{\text{CC2}}(\bar{t},\ t,\ \bar{\kappa},\ \kappa,\ \bar{E}^{f},\ E^{f},\ \bar{\omega}^{f}) + \frac{1}{2}\sum_{\mu} Q_{\mu}(\mathbf{D}^{\text{CC2},f,\text{eff}})\cdot V_{\mu}(\mathbf{D}^{\text{CC2},f,\text{eff}}) \tag{38}$$

Because of the importance of the excitonic coupling to a polarizable environment for the excitation energies of bright states and the correct ordering of the excited states, we implemented the possibility of including the first- and second-order LR contributions to the Jacobian matrix. Following Lunkenheimer and Köhn,[21] we count the interaction with the environment like the electron fluctuation potential as a first-order operator. Also, the double excitation operator, $\hat{T}_2$, built from the CC2 amplitudes is counted as the first-order operator. In the derivation of the CC2 model for the vacuum case,[20] the ground-state singles amplitudes were treated as zeroth-order quantities to arrive at ground-state cluster equations with a Jacobian that gives excitation energies that are correct through second order. To maintain the simplicity of the Lagrange functional for the excited-state total energy, we count, however, for the derivation of the LR contribution the ground-state singles amplitudes and Lagrange multipliers as in the Møller−Plesset perturbation theory[26] as second-order quantities, assuming a closed-shell or spin-unrestricted reference determinant. With

https://doi.org/10.1021/acs.jpca.5c02873
J. Phys. Chem. A XXXX, XXX, XXX−XXX

these assumptions, we get, as for ADC(2), only in the singles/singles block of the Jacobian matrix, an additional LR contribution

$$\mathbf{A}^{\mathrm{CC2,rsp}}_{ai,ck} = \sum_{\lambda} \langle {}^{a}_{i}|\widehat{\widetilde{V}}_{\lambda} + [\widehat{\widetilde{V}}_{\lambda},\ \widehat{T}_2]|\mathrm{HF}\rangle \times \langle \mathrm{HF}|[\hat{\hat{Q}}^{\mathrm{fast}}_{\lambda},\ E_{ck}]|\mathrm{HF}\rangle \tag{39}$$

To distinguish them from the pure PTED coupling scheme, we denote the generalization, which includes the additional LR contributions in the secular matrix, as PTED(LR).

In contrast to the post-SCF coupling scheme,[18] the secular matrix for PTED(LR)-CC2 does, with the above LR contribution, not depend on ground-state multipliers, so that the Lagrange function for the excited-state total energy does not involve more variables than for the vacuum case. PTED-COSMO-MP2, PTED-COSMO-ADC(2), and PTED(LR)-COSMO-ADC(2) energies had already been implemented by Lunkenheimer and Köhn[21] in the `ricc2` program[42] of the TURBOMOLE package.[43] As part of the current work, we extended this implementation to COSMO-CC2, and for MP2, ADC(2), and CC2, we also cover PE.

Gradients for Ground and Excited States. As pointed out above, the PTED variants where the reaction field potential is equilibrated with the orbital-relaxed density of the solute's reference state have the advantage that the respective orbital-relaxed Lagrange function for the total energy of the reference is stationary after convergence of the SCRF iterations. This advantage is maintained in the PTED(LR) coupling scheme for the excitation energies. As a consequence, analytical nuclear gradients can be computed straightforwardly.

For the pure PTED coupling scheme without LR contributions, the nuclear gradients require, in addition to the contributions present in the vacuum case, only the derivative of the polarization contribution to the total energy. For COSMO, the polarization contribution to the total energy is (vide supra):

$$L^{\mathrm{pol}}_{\mathrm{COSMO}} = \frac{1}{2}\sum_{\nu} Q_{\nu}(\mathbf{D})\cdot V_{\nu}(\mathbf{D}) \tag{40}$$

where **D** is the orbital-relaxed density for the reference state. Its first derivative w.r.t. a nuclear coordinate x is

$$\frac{\partial L^{\mathrm{pol}}_{\mathrm{COSMO}}}{\partial x} = \sum_{\mu} Q_{\mu}(\mathbf{D})\Big(V^{[x],\mathrm{nuc}}_{\mu} + \sum_{\alpha\beta} D_{\alpha\beta}V^{[x]}_{\alpha\beta,\mu}\Big) - \sum_{\alpha\beta} F^{\mathrm{eff,pol}}_{\alpha\beta}S^{[x]}_{\alpha\beta} - \frac{1}{f(\epsilon)}\frac{1}{2}\sum_{\mu\nu} Q_{\mu}(\mathbf{D})\frac{\partial \mathcal{A}^{\mathrm{COSMO}}_{\mu\nu}}{\partial x}Q_{\nu}(\mathbf{D}) \tag{41}$$

with

$$F^{\mathrm{eff,pol}}_{\alpha\beta} = \frac{1}{2}\sum_{r}\sum_{pq} C_{\alpha p}C_{\beta q}(D_{pr}G_{rq}(\mathbf{D}) + D_{rq}G_{pr}(\mathbf{D})) \tag{42}$$

Above, α and β refer to atomic orbitals, $V^{[x]}_{\alpha\beta,\mu}$ are the first derivatives w.r.t. x of the potential energy integrals for a cavity surface site μ, and $S^{[x]}_{\alpha\beta}$ are the derivatives of the overlap integrals. $V^{[x],\mathrm{nuc}}_{\mu}$ is the first derivative of the potential at site μ due to the solute's nuclear charges, and $C_{\alpha p}$ are the MO coefficients. The equations for L^{pol}_{COSMO} and its derivatives with respect to nuclear coordinates have—for the pure PTED coupling scheme with orbital-relaxed densities—the same structure for all electronic structure methods for ground and electronically excited states. The quantity that depends on the method and state is the density **D**.

To evaluate for the PTED(LR) variants of COSMO-ADC(2) and COSMO-CC2 the additional LR contribution to the Lagrangian for excited reference states, we introduce auxiliary densities. For CC2, they are defined as

$$D^{\xi,f} = \langle \overline{E}^{f}_{1}|e^{-T_1}E_{pq}e^{T_1}|\mathrm{HF}\rangle + \langle \overline{E}^{f}_{1}|[E_{pq},\ \widehat{T}_2]|\mathrm{HF}\rangle \tag{43}$$

$$D^{\eta,f} = \langle \mathrm{HF}|[E_{pq},\ \widehat{E}^{f}_{1}]|\mathrm{HF}\rangle \tag{44}$$

For ADC(2), they are defined correspondingly but without similarity transformation with T_1. With these densities, the LR contribution to the Lagrangian can be written as

$$L^{\mathrm{LR}}_{\mathrm{COSMO}} = \sum_{\mu} Q^{\mathrm{fast}}_{\mu}(\mathbf{D}^{\xi,f})\cdot V_{\mu}(\mathbf{D}^{\eta,f}) \tag{45}$$

We note that the charges for the LR contribution are evaluated with the scaling factor for optical frequencies, $f(n^2)$. The first derivatives of the LR contribution are

$$\frac{\partial L^{\mathrm{LR}}_{\mathrm{COSMO}}}{\partial x} = \sum_{\mu} Q^{\mathrm{fast}}_{\mu}(\mathbf{D}^{\xi,f})\sum_{\alpha\beta} D^{\eta,f}_{\alpha\beta}V^{[x]}_{\alpha\beta,\mu} + \sum_{\mu} Q^{\mathrm{fast}}_{\mu}(\mathbf{D}^{\eta,f})\sum_{\alpha\beta} D^{\xi,f}_{\alpha\beta}V^{[x]}_{\alpha\beta,\mu} - \sum_{\alpha\beta} F^{\mathrm{eff,LR}}_{\alpha\beta}S^{[x]}_{\alpha\beta} - \frac{1}{f(n^2)}\sum_{\mu\nu} Q^{\mathrm{fast}}_{\mu}(\mathbf{D}^{\xi,f})\frac{\partial \mathcal{A}^{\mathrm{COSMO}}_{\mu\nu}}{\partial x}Q^{\mathrm{fast}}_{\nu}(\mathbf{D}^{\eta,f}) \tag{46}$$

with

$$F^{\mathrm{eff,LR}}_{\alpha\beta} = \frac{1}{2}\sum_{r}\sum_{pq} C_{\alpha p}C_{\beta q}(D^{\xi,f}_{pr}G^{fast}_{rq}(\mathbf{D}^{\eta,f}) + D^{\xi,f}_{rq}G^{fast}_{pr}(\mathbf{D}^{\eta,f})) + \frac{1}{2}\sum_{r}\sum_{pq} C_{\alpha p}C_{\beta q}(D^{\eta,f}_{pr}G^{fast}_{rq}(\mathbf{D}^{\xi,f}) + D^{\eta,f}_{rq}G^{fast}_{pr}(\mathbf{D}^{\xi,f})) \tag{47}$$

For PE, the interaction with the environment includes, in addition to the polarization contribution, an electrostatic contribution plus possibly mechanical contributions such as Lennard-Jones potentials (vide supra) that depend only on the positions of the nuclei.

$$L^{\mathrm{emb}}_{\mathrm{PE}} = L^{\mathrm{pol}}_{\mathrm{PE}} + L^{\mathrm{es}}_{\mathrm{PE}} + L^{\mathrm{ECP}}_{\mathrm{PE}} + L^{\mathrm{MM}}_{\mathrm{PE}} \tag{48}$$

The mechanical contribution to the Lagrangian, $L^{\mathrm{MM}}_{\mathrm{PE}}$, and its contribution to nuclear gradients do not depend on the electronic structure method and the reaction field coupling scheme. Also, the ECP contributions to energies and gradients do not depend on the coupling scheme and only implicitly through the electron density on the electronic structure method. Therefore, we will not further discuss these two contributions in the current work but refer to refs 19,29. The electrostatic interaction energy and its contribution to nuclear gradients can be evaluated with the orbital-relaxed density matrix in the atomic orbital basis as

https://doi.org/10.1021/acs.jpca.5c02873
J. Phys. Chem. A XXXX, XXX, XXX−XXX

Table 1. Results for the Structures of DMABN with COSMO-CC2/def2-TZVPP within the PTED(LR) Coupling Scheme

	vacuum	n-C_6H_{14}	C_6H_6	$CHCl_3$	C_6H_5Cl	CH_2Cl_2	CH_3CN	$(CH_3)_2SO$
				TICT state				
ϕ (°)[a]	42	37	35	27	26	1	0	0
d(C_1C_2)[d]	143.0	143.4	143.5	143.9	144.0	144.5	144.6	144.6
d(C_2C_3)[d]	137.3	137.3	137.3	137.4	137.5	137.7	137.8	137.8
d(C_3C_4)[d]	144.7	144.1	143.9	143.2	143.0	142.0	141.8	141.8
d(C_4N)[d]	144.3	144.1	144.0	143.6	143.5	143.0	143.1	143.1
dipole [D]	13.3	15.5	16.1	18.4	18.8	20.2	21.3	21.4
				LE state[e]				
τ (°)[b]	19	18	18	19	19	20	23	23
d(C_1C_2)[d]	141.3	141.1	141.0	140.8	140.8	140.7	140.5	140.5
d(C_2C_3)[d]	143.6	143.8	143.9	144.3	144.4	144.6	144.7	144.7
d(C_3C_4)[d]	141.6	141.3	141.2	140.7	140.6	140.4	140.1	140.2
dipole [D]	10.1	11.7	12.2	15.7	15.9	16.4	17.3	17.3
				ground state				
ω (°)[c]	24	23	23	21	21	20	18	18
d(C_3C_4)[d]	141.4	141.5	141.6	141.7	141.7	141.8	141.9	141.9
d(C_4N)[d]	137.8	137.5	137.4	137.1	137.0	136.8	136.6	136.5
dipole [D]	7.4	8.2	8.5	9.3	9.5	9.8	10.3	10.4

[a]Out-of-plane angle of the dimethylamino group, defined as the angle between the C_4N bond and the plane containing the atoms C_4, C_3, and $C_{3'}$, for the LE and the ground state 0° in all environments. [b]Twist angle of the dimethylamino group, defined as the average of the dihedral angles C_3C_4NMe and $C_{3'}C_4NMe'$, for the TICT state 90° and the ground state 0° in all environments. [c]Wagging angle of the dimethylamino group, defined as the angle between the C_4N bond and the plane containing the N atom and the two methyl C atoms, for the LE and TICT states <1° in all environments. [d]Bond distance in pm. [e]Norm of remaining gradients: $CHCl_3$ 7×10^{-5} a.u., C_6H_6Cl 1×10^{-4} a.u., CH_2Cl_2 2×10^{-4} a.u., CH_3CN 4×10^{-4} a.u., and $(CH_3)_2SO$ 5×10^{-4} a.u.

$$L_{\mathrm{PE}}^{\mathrm{es}} = \sum_u Q_u^{\mathrm{es}} \left(V_u^{\mathrm{nuc}} + \sum_{\alpha\beta} D_{\alpha\beta} V_{\alpha\beta,u} \right) \tag{49}$$

$$\frac{\partial L_{\mathrm{PE}}^{\mathrm{es}}}{\partial x} = \sum_u Q_u^{\mathrm{es}} \left(V_u^{[x],\mathrm{nuc}} + \sum_{\alpha\beta} D_{\alpha\beta} V_{\alpha\beta,u}^{[x]} \right) - \sum_{\alpha\beta} F_{\alpha\beta}^{\mathrm{eff,es}} S_{\alpha\beta}^{[x]} \tag{50}$$

with

$$F_{\alpha\beta}^{\mathrm{eff,es}} = \frac{1}{2} \sum_r \sum_{pq} C_{\alpha p} C_{\beta q} (D_{pr} G_{rq}^{\mathrm{es}} + D_{rq} G_{pr}^{\mathrm{es}}) \tag{51}$$

It does not depend on the reaction field coupling scheme. For the PTED coupling scheme with the reaction field equilibrated with the orbital-relaxed density of the reference state, the polarization contribution to the Lagrangian and its contribution to the nuclear gradients become for the PE:

$$L_{\mathrm{PE}}^{\mathrm{pol}} = -\frac{1}{2} \sum_{uv} \left(V_u(\mathbf{D}) + V_u^{\mathrm{es}} \right) R_{uv} \left(V_v(\mathbf{D}) + V_u^{\mathrm{es}} \right) \tag{52}$$

$$\frac{\partial L_{\mathrm{PE}}^{\mathrm{pol}}}{\partial x} = \sum_u Q_u^{\mathrm{ind}}(\mathbf{D}) \left(V_u^{[x],\mathrm{nuc}} + \sum_{\alpha\beta} D_{\alpha\beta} V_{\alpha\beta,u}^{[x]} \right) - \sum_{\alpha\beta} F_{\alpha\beta}^{\mathrm{eff,pol}} S_{\alpha\beta}^{[x]} \tag{53}$$

The expression for $F_{\alpha\beta}^{\mathrm{eff,pol}}$ has, for the atomistic PE, the same form as for COSMO, if expressed through the induced reaction field operator, $\hat{G}(\mathbf{D})$. The electrostatic contribution to the gradient can be combined with the polarization contribution by adding Q_u^{es} to Q_u^{ind} and $\mathbf{G}^{\mathrm{es}}$ to $\mathbf{G}(\mathbf{D})$. The additional LR contributions for the PTED(LR) variants of PE-ADC(2) and PE-CC2 are

$$L_{\mathrm{PE}}^{\mathrm{LR}} = -\sum_{uv} V_u(\mathbf{D}^{\xi,f}) R_{uv} V_v(\mathbf{D}^{\eta,f}) \tag{54}$$

$$\frac{\partial L_{\mathrm{PE}}^{\mathrm{LR}}}{\partial x} = \sum_u Q_u^{\mathrm{ind}}(\mathbf{D}^{\xi,f}) \sum_{\alpha\beta} D_{\alpha\beta}^{\eta,f} V_{\alpha\beta,u}^{[x]} + \sum_u Q_u^{\mathrm{ind}}(\mathbf{D}^{\eta,f}) \sum_{\alpha\beta} D_{\alpha\beta}^{\xi,f} V_{\alpha\beta,u}^{[x]} - \sum_{\alpha\beta} F_{\alpha\beta}^{\mathrm{eff,LR}} S_{\alpha\beta}^{[x]} \tag{55}$$

The above expressions for the gradients of the PTED variants of MP2, ADC(2), and CC2 and for the PTED(LR) variants of ADC(2) and CC2 have been implemented in a development version of the TURBOMOLE package.[43,44]

RESULTS AND DISCUSSION

CT State of DMABN in Solution. DMABN is a prototypical chromophore for dual fluorescence that has been extensively studied in the literature, both experimentally and theoretically (see, e.g., refs 45,46 and references cited therein). After photoexcitation into the bright $S_2(^1L_a)$ state, DMABN decays rapidly to the locally excited $S_1(^1L_b$, LE) minimum on the S_1 potential energy surface from where it can either decay directly to the ground or a triplet excited state or decompose or, depending on the polarity of the environment, relax to a twisted intramolecular charge-transfer $S_1(^1L_a$, TICT) minimum with a large Stokes shift and dipole moment.[45]

The relative energies of the LE and TICT minima and details of the TICT equilibrium geometry are known to depend crucially on the electronic structure level, the polarity of the environment, and how the latter is accounted for in the electronic structure calculation.[46] Köhn and Hättig found at the CC2/TZVPP level in the gas phase for the LE state a C_2-symmetric minimum and for the TICT state a C_{2v}-symmetric saddle point and a C_s-symmetric minimum where the amino group is tilted by 41° out of the phenyl ring plane.[47] Single-point

https://doi.org/10.1021/acs.jpca.5c02873
J. Phys. Chem. A XXXX, XXX, XXX−XXX

Table 2. Results for the Energies of DMABN with COSMO-CC2/def2-TZVPP within the PTED(LR) Coupling Scheme[a]

	vacuum	n-C_6H_{14}	C_6H_6	$CHCl_3$	C_6H_5Cl	CH_2Cl_2	CH_3CN	$(CH_3)_2SO$
				TICT state				
ΔE[b] [eV]	2.49 (2.89)	2.42 (2.83)	2.39 (2.81)	2.20 (2.62)	2.19 (2.61)	2.23 (2.64)	1.95 (2.36)	1.97 (2.39)
$\tilde{\nu}_{max}$[f] [eV]						2.83	2.52	
T_e[d] [eV]	4.06 (4.45)	3.88 (4.28)	3.82 (4.23)	3.64 (4.04)	3.61 (4.01)	3.54 (3.93)	3.41 (3.81)	3.40 (3.80)
				LE state[e]				
ΔE[b] [eV]	3.78 (3.88)	3.70 (3.82)	3.67 (3.80)	3.52 (3.70)	3.50 (3.68)	3.42 (3.62)	3.27 (3.49)	3.27 (3.50)
$\tilde{\nu}_{max}$[f] [eV]		3.65				3.49	3.42	
T_e[d] [eV]	4.14 (4.25)	4.06 (4.20)	4.03 (4.18)	3.96 (4.16)	3.95 (4.15)	3.92 (4.15)	3.87 (4.13)	3.87 (4.12)
				ground state				
$\Delta E(S_2)$[c] [eV]	4.77 (4.91)	4.57 (4.71)	4.52 (4.65)	4.45 (4.58)	4.42 (4.55)	4.41 (4.53)	4.38 (4.50)	4.35 (4.46)
$\Delta E(S_1)$[c] [eV]	4.42 (4.45)	4.35 (4.39)	4.33 (4.37)	4.31 (4.36)	4.29 (4.35)	4.29 (4.35)	4.28 (4.34)	4.26 (4.32)

[a]Estimated CC3 results are given in parentheses. [b]Vertical fluorescence energy. [c]Vertical excitation energy. [d]Adiabatic excitation energy relative to the ground-state minimum. [e]Norm of remaining gradients; see Table 1. [f]Experimental fluorescence maxima from ref 49.

CCSDR(3)/SVP calculations confirmed that in the gas phase, the energy of the tilted structure is about 0.1 eV below that of the C_{2v}-symmetric saddle point. In the point group C_2, the LE (^1L_b) state belongs to the B irreducible representation (irrep) and the ICT (^1L_a) state to the A irrep, so that the contributing electronic configurations cannot mix unless the molecular structure is distorted out of the C_2 symmetry. For CASSCF, the out-of-plane angle and the energy difference between the tilted and nontilted structures depend on the active space and whether state-averaging is employed or not.[47] At the multireference configuration interaction singles level with 8 electrons and 7 orbitals in the active space, the TICT minimum has a structure close to the C_{2v}-symmetric saddle point of CC2/TZVPP without out-of-plane tilting of the amino group.[46] Also, TDDFT/B3LYP yields in the gas phase[48] a TICT minimum with C_{2v} symmetry.

Since the CC2/TZVPP calculations in the gas phase gave a larger dipole moment at the C_{2v}-symmetric saddle point than at the TICT minimum, it was already conjectured in ref 47 that the C_{2v} structure will become a minimum in sufficiently polar solvents. This was in ref 21 corroborated by single-point COSMO-ADC(2)/TZVPP calculations at the CC2/TZVPP gas phase structures within the PTED(LR) coupling scheme, and the reaction field fully equilibrated for the TICT state, which gave in acetonitrile a lower energy at the C_{2v} structure than at the tilted C_s structure, while in hexane, the C_s structure still had the lower energy. With the post-SCF coupling scheme, which equilibrates the reaction field with the ground state and includes in addition only the LR contributions, a full geometry optimization at the COSMO-ADC(2)/def2-TZVPP level gave in acetonitrile a tilted TICT minimum with an out-of-plane angle of 32°, only slightly smaller than in the gas phase.[18] In addition, the amino group was only partially twisted relative to the phenyl ring (τ = 56°), which was attributed to the missing SS contributions in the post-SCF coupling scheme.

Table 1 summarizes the results obtained for the structure of DMABN in vacuum and with the PTED(LR) coupling scheme in seven solvents of different polarities at the CC2/def2-TZVPP level. As anticipated, we observe indeed for the TICT minimum a decrease in the out-of-plane angle (ϕ) of the amino group with increasing solvent polarity until it reaches 0° in acetonitrile. The pyramidalization at the C_4 atom decays quickly from 26° in chlorobenzene (ϵ_r = 5.69) to 1° in dichloromethane (ϵ_r = 8.93). The twist (τ) angle for the TICT minimum remains with the PTED(LR) coupling scheme in all solvents at 90°. Of the bond lengths in the phenyl ring, $d(C_3C_4)$ shows with −2.9 pm the largest change from vacuum to acetonitrile, while the other bond lengths in the phenyl ring, $d(C_1C_2)$ and $d(C_2C_3)$, slightly increase with the polarity. For the LE state, a minimum could be found at the PTED(LR)-CC2/def2-TZVPP level only in vacuum and the nonpolar solvents n-hexane and benzene. In chloroform and more polar solvents, the LE minimum turned to a flat region on the potential energy surface with a very small but nonvanishing remaining gradient (see Table 1) from where the structure can convert without barrier to the TICT minimum. This is related to an underestimation of the energy of the TICT minimum relative to that of the LE minimum at the CC2 level (vide infra). For the LE and the ground state, $d(C_3C_4)$ increases and $d(C_4N)$ shortens with the polarity of the solvent as a result of increasing conjugation between the amino lone pair with the π-system, which is associated with an increase of the dipole moment. In the ground state, the increased conjugation also leads to a flattening of the dimethylamino group, i.e., a decrease of the wagging angle ω (see Table 1).

The results for the adiabatic energy differences between the ground and the excited-state minima (T_e) show the expected shifts with polarity: while in the gas phase, CC2 predicts the TICT minimum 0.08 eV below the LE minimum, this energy difference increases in solution from 0.18 eV in n-hexane to 0.47 eV in dimethyl sulfoxide (DMSO). That CC2 predicts the CT minimum to be already in the gas phase below the LE minimum is due to missing higher-order correlation effects. In ref 47, these correlation contributions were estimated from the difference between CC2/SVP and CCSDR(3)/SVP results. Adding this correction and including the zero-point vibrational energy resulted in the estimate that in the gas phase the CT minimum is ≈ 0.17 eV above the LE minimum. For the current work, we estimated the higher-order correlation effects as the sum of a CC2 → CCSD correction computed in the def2-TZVPP basis with all virtual MOs included and a CCSD → CC3 correction calculated in a restricted virtual space (RVS) with the highest 275 virtual MOs excluded from the correlated calculation, corresponding to a cutoff of ≈ 2 E_h. For the calculations in solution, we accounted for the solvent effects by including also for the calculation of the corrections the (static) reaction field as equilibrated at the PTED-CC2 level for the respective reference state in the Hamiltonian, but no LR and nonequilibrium contributions as they are not yet available for CCSD and CC3. These calculations were done with a development version of TURBOMOLE's ccsdf12 program. The PTED(LR)-CC3 excitation energies were then estimated as

https://doi.org/10.1021/acs.jpca.5c02873
J. Phys. Chem. A XXXX, XXX, XXX−XXX

$$E^{\mathrm{est}}_{\mathrm{PTED(LR)\text{-}CC3}} = E_{\mathrm{PTED(LR)\text{-}CC2}} + [E_{\mathrm{PTED_{CC2}\text{-}CCSD}} - E_{\mathrm{PTED\text{-}CC2}}] + [E_{\mathrm{PTED_{CC2}\text{-}CC3_{RVS}}} - E_{\mathrm{PTED_{CC2}\text{-}CCSD_{RVS}}}] \quad (56)$$

The results are collected in Table 2. At this level, the energy difference T_e(TICT) − T_e(LE) becomes in the gas phase 0.20 eV instead of the −0.08 eV obtained with CC2 and remains positive also in the nonpolar solvents *n*-hexane and benzene. Only in chloroform and other polar solvents does the TICT minimum become lower in energy than the LE minimum. The change of T_e(TICT) − T_e(LE) from CC2 to CC3 originates from a blue shift of ≈0.4 eV of the S_1 excitation energies at the TICT minimum from CC2 to CC3. At the LE minimum, the S_1 excitation energy increases from CC2 to CC3 only by 0.11 eV (gas phase) to 0.25 eV (DMSO), while at the ground-state structure, the CC2 excitation energies for S_1 and S_2 agree within, respectively, ≤0.06 and ≤0.14 eV with the CC3 results. The vertical deexcitation energies at the LE minimum are in reasonable agreement with the experimental fluorescence maxima. For the TICT minimum, however, this is only the case for the CC3 results.

CT State of DMABN Complexed by Curcurbit[7]uril. As a test case for the gradients of the PTED(LR) variants of PE-MP2 and PE-ADC(2), we reinvestigate the host−guest complex of DMABN inside curcurbit[7]uril (CB[7]). This complex was used in ref 19 as test case for the analytic excited-state gradients for PE-ADC(2) with the post-SCF coupling scheme. For the current work, it is particularly interesting how much the results obtained with the PTED(LR) coupling scheme for the TICT state differ from those obtained with the post-SCF coupling scheme. The CB[7] host provides a relatively rigid and only modestly polar environment for guest molecules,[50] where long-range polarization effects and, thus, the differences between the PTED(LR) and the post-SCF coupling schemes should be less important than in polar solvents.

We followed a similar computational protocol as used in ref 19. The geometry of the host CB[7] was taken from the structure for the DMABN·CB[7] complex optimized for its ground state in a supermolecular RI-MP2 calculation in the cc-pVDZ orbital and auxiliary basis sets[51,52] with frozen $1s^2$ occupations at all non-hydrogen atoms.[19] The same distributed multipole moments, dipole−dipole polarizabilities, and Lennard-Jones potentials as in ref 19 were used to represent CB[7] in the PE calculations. We augmented this potential by all-electron ECPs from ref 29 to account for the Pauli repulsion in the electron-structure calculation and avoid electron spill-out from the QM system. This allowed us to use basis sets with diffuse functions (vide infra).

With this setup for the environment, we optimized the geometry for DMABN inside CB[7] for the ground state with MP2 and for S_1 with ADC(2) using the def2-TZVPP orbital and auxiliary basis sets[53,54] and the frozen core approximation for the $1s^2$ orbitals at C and N. At the optimized geometries, we performed in addition single-point calculations for the excitation energies in the larger aug-cc-pVTZ basis sets.[51,52,55] For comparison, we performed these calculations with the PTED-(LR) and the post-SCF coupling scheme. The latter reduces for MP2 to the PTE (perturbation through the energy) coupling scheme.

The results for the equilibrium geometries of DMABN in the S_1 TICT and the ground state are summarized in Table 3. For

Table 3. Structure of DMABN inside the CB[7] Host in the S_1 TICT and the Ground State in Comparison to the Gas Phase[a]

	DMABN·CB[7]		DMABN
	PTED	post-SCF	gas phase
TICT state			
ϕ[b]	49	49	41
τ[c]	57	55	90
d(C_1C_2)[d]	142.3	142.3	142.8
d(C_2C_3)[d]	136.7	136.7	137.1
d(C_3C_4)[d]	143.9	144.1	144.5
d(C_4N)[d]	145.3	144.7	144.3
$\Delta E(S_1)$[f] [eV]	2.26 (2.72)	2.29 (2.60)	2.44 (2.80)
$\tilde{\nu}^{\mathrm{em}}_{\mathrm{max}}$[g]	2.51		
ground state			
ω[e]	36	36	26
d(C_3C_4)[d]	140.6	140.6	141.0
d(C_4N)[d]	139.7	139.7	137.9
$\Delta E(S_1)$[f] [eV]	4.59 (4.45)	4.59 (4.44)	4.38 (4.38)
$\tilde{\nu}^{\mathrm{abs}}_{\mathrm{max}}$[h]	4.10		
$\Delta E(S_2)$[f] [eV]	4.68	4.68	4.60

[a]Calculations were done at the ADC(2)/def2-TZVPP level for S_1 and MP2/def2-TZVPP for S_0, and the CB[7] host has been approximated by a polarizable embedding combined with the PTED and post-SCF coupling scheme. [b]Out-of-plane angle of the dimethylamino group, defined as the angle between the C_4N bond and the plane containing the atoms C_4, C_3, and $C_{3'}$. [c]Twist angle of the dimethylamino group, defined as the average of the dihedral angles C_3C_4NMe and $C_{3'}C_4$NMe′. [d]Bond distance in pm. [e]Wagging angle of the dimethylamino group, defined as the angle between the C_4N bond and the plane containing the N atom and the two methyl C atoms. [f]Computed ADC(2)/aug-cc-pVTZ vertical transition energy. [g]Emission band maximum of DMABN·CB[7] in aqueous solution from ref 56. [h]Absorption band maximum of DMABN·CB[7] in aqueous solution from ref 56.

the ground state, we find no significant differences between the equilibrium structures obtained for DMABN·CB[7] with the simple PTE and the more costly PTED reaction field coupling scheme—within the digits given in Table 3, the structures are identical. Similarly, we find that the PTED(LR) and post-SCF results for the absorption energies at the ground-state structure and with the ground-state reaction field agree within 0.01 eV. In the TICT state, this is not the case for all coordinates. In particular, for the C_4−N bond distance, the structures obtained with the PTED(LR) coupling scheme differ by 0.4 pm from the result obtained with the post-SCF coupling scheme. However, the PTED(LR) result with ADC(2)/aug-cc-pVTZ for the emission energy from S_1 is only 0.03 eV below the respective post-SCF value. Both underestimate the experimental fluorescence band maximum by 0.2−0.25 eV, likely mostly due to the remaining electronic structure error at the ADC(2) level. To correct for this, we estimated the change in the excitation energy from ADC(2) to CC3 in the def2-TZVPP basis. Thereby, we included for the correction of the PTED result the static reaction field as equilibrated at the PTED-ADC(2) level and for the correction of the post-SCF result the static Hartree−Fock reaction field. Similar as in solution, the estimated CC3 results for the deexcitation energies from the TICT state are about 0.31−0.46 eV higher than those obtained with the second-order method. For DMABN in CB[7], they overestimate the experimental result, which might be partially due to the aqueous solution that was used in the experiment but is neglected in the current calculations. Overall, the differences between the

https://doi.org/10.1021/acs.jpca.5c02873
J. Phys. Chem. A XXXX, XXX, XXX−XXX

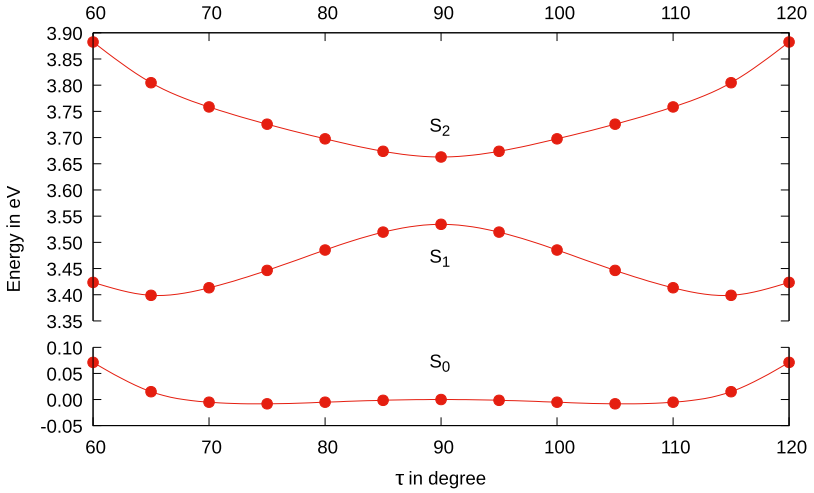


Figure 1. Potential energy curves of S_0, S_1, and S_2 in C9A along the torsion angle τ computed at the MP2/cc-pVDZ (ground state) and ADC(2)/cc-pVDZ (excited states) levels. Unrelaxed scan started from the optimized MP2/cc-pVDZ structure for S_0 at $\tau = 90°$. Energies are given in eV relative to the ground-state energy at $\tau = 90°$.

Table 4. Vertical Excitation Energies, Dipole Moments (μ), and Torsion Angle (τ) Computed at the PTED(LR)-ADC(2)/aug-cc-pVTZ Level for the PTED-MP2/def2-TZVPP Optimized Ground-State Structures[a]

solvent	ϵ_r	τ (°)	$\mu(S_0)$	$\Delta E(S_1)$	$\tilde{\nu}_{max}^{abs}$ [d]	$\mu(S_1)$	$\Delta E(S_2)$	$\mu(S_2)$
vacuum	1.00	71	1.97	3.25	3.25[e]	5.52	3.56	2.54
perfluorohexane	1.57	71	2.16	3.22	3.28	3.99	3.53	3.62
n-hexane	1.89	72	2.23	3.22	3.23	3.38	3.51	4.06
triethylamine	2.42	72	2.32	3.23	3.21	2.87	3.51	4.33
benzene	2.28	72	2.30	3.22	3.19	2.80	3.50	4.45
1,4-dioxane	2.22	72	2.29	3.22	3.19	2.99	3.51	4.30
chloroform	4.81	72	2.52	3.25	3.20	1.82	3.52	4.83
chlorobenzene	5.69	73	2.58	3.25	3.18	1.46	3.50	5.09
dichloromethane	8.93	73	2.67	3.27	3.19	1.20	3.52	5.12
acetonitrile	36.6	73	2.80	3.29	3.21	0.74	3.54	5.25
DMA[b]	37.8	73	2.80	3.28	3.19	0.59	3.53	5.38
DMSO[c]	47.2	73	2.81	3.28	3.17	0.50	3.52	5.45

[a]Dipole moments are in Debye, and excitation energies and band maxima are in eV. [b]*N*,*N*-dimethylacetamide. [c]Dimethyl sulfoxide. [d]Experimental absorption band maxima from ref 59. [e]Fluorescence excitation maximum from ref 57.

structures obtained with the two coupling schemes are small for this system.

Delocalized S_1 State of C9A in Solution. Similar to DMABN, C9A also shows in polar solvents fluorescence from a TICT state with a large Stokes shift. But otherwise, the electronic structure of the lowest two singlet excited states and their interplay is quite different from the situation in DMABN. Along the twisting coordinate τ, the ground-state potential energy surface of C9A is very shallow between $60° < \tau < 120°$ (cf. Figure 1). At the MP2/def2-TZVPP level, the fully twisted structure with $\tau = 90°$ is a saddle point, but only 1.46 kJ/mol (0.015 eV) higher in energy than the C_2-symmetric minima at $\tau = 90 \pm 19°$. This fits qualitatively to the tiny barrier height of 17 cm^{-1} (0.2 kJ/mol) deduced in ref 57 from laser-induced fluorescence spectra in a supersonic jet. At the idealized fully twisted C_{2v}-symmetric ground-state structure, the lowest two singlet excitations are $1\ ^1A_2$ (S_1) and $2\ ^1A_1$ (S_2). The first one, $1\ ^1A_2$, is an ICT transition from the carbazole HOMO−1 to the anthracene LUMO, and the second one, $2\ ^1A_1$ (S_2), is a local HOMO-to-LUMO transition within the anthracene group. At C_{2v} symmetry, the ICT transition is dark (dipole forbidden), while the $2\ ^1A_1$ transition is bright with an oscillator strength of 0.2. In contrast to the local and ICT transitions in DMABN, the two lowest states in C9A both belong to the totally symmetric irreducible representation of C_2 for $\tau \neq 90°$ and mix strongly with each other.[58] This configuration mixing stabilizes the lower and destabilizes the upper state with increasing deviation of τ from 90°, and both excitations become delocalized (DE) with a partial CT character. The S_1 potential has, along the twist angle τ, a double minimum shape with a maximum at 90°, while the S_2 potential curve has a single minimum at 90° (cf. Figure 1). The barrier on the S_1 potential is much larger than in the ground state, ≈ 0.15 eV in the unrelaxed scan shown in Figure 1. The MP2 and ADC(2) potential energy curves agree qualitatively with those obtained by Evers et al. with DFT/MRCI along a relaxed scan on the HF-SCF ground-state potential,[58] although ADC(2) gives a larger S_1-S_2 energy gap at $\tau = 90°$. Because of the strong interaction between the ICT and LE configurations, C9A does not show dual fluorescence like DMABN does in polar solvents but a fluorescence signal with a nonlinear increase of the Stokes shift with solvent polarity.[59]

In Table 4, we compile the results obtained for the vertical excitation energies with PTED(LR)-ADC(2)/aug-cc-pVTZ at the ground-state structures optimized in solution at the PTED-MP2/def2-TZVPP level. The ground-state structure remains almost unchanged when the environment is changed from

https://doi.org/10.1021/acs.jpca.5c02873
J. Phys. Chem. A XXXX, XXX, XXX−XXX

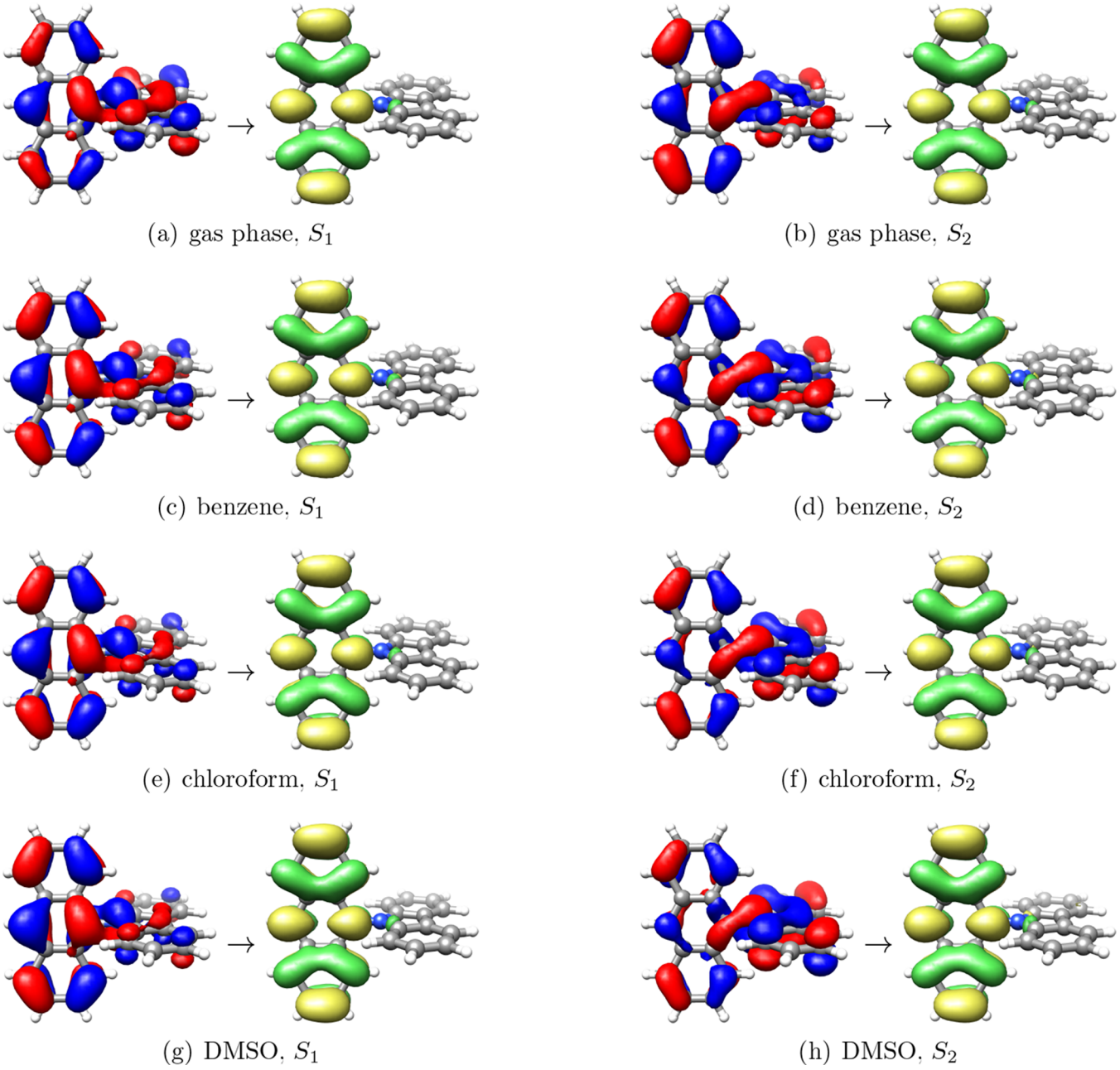


Figure 2. Natural transition orbitals for C9A from ADC(2)/aug-cc-VTZ calculation at the MP2/def2-TZVPP optimized ground-state geometries, using in solution the PTED(LR) coupling scheme. For each environment and state, the occupied NTO is shown on the left side in blue and red and the virtual NTO on the right side in green and yellow.

vacuum to polar solvents. The torsion angle between the anthracene and the carbazole groups increases only marginally from 71 to 73°, and the ground-state dipole moment increases only slightly from 2.0 to 2.8 D. The computed vacuum value for the twist angle at the S_0 equilibrium structure agrees well with the value of 77.5° that has in ref 57 been deduced from a potential fitted to fluorescence excitation spectra recorded in a supersonic jet. Also, the vertical excitation energies to S_1 and S_2 change with a few hundredths of an eV only very little with the solvent polarity, which is in line with the experimental results[59] for the absorption band maxima. While the latter slightly decrease with solvent polarity, the computed results slightly increase. However, the deviations are $\lesssim$ 0.1 eV below the intrinsic accuracy of ADC(2) and the comparison between vertical excitation energies and band maxima. The slight increase of the computed vertical excitation energies with solvent polarity is in line with the fact that the excited-state dipole moments for S_1 and S_2 have the opposite direction of the ground-state dipole moment. Thus, S_1 and S_2 are slightly destabilized by the reaction field potential equilibrated with the ground-state charge distribution.

Despite the very small changes of the excitation energies with solvent polarity, the natural transition orbitals (NTOs) and the excited-state dipole moments found at the ground-state structure for S_1 and S_2, shown in Figure 2, change significantly with increasing dielectric constant of the solvent. In vacuum, the NTOs show for S_1 a larger CT contribution than for S_2. Also, the dipole moment of S_1 is more than twice as large as that of S_2. In

https://doi.org/10.1021/acs.jpca.5c02873
J. Phys. Chem. A XXXX, XXX, XXX−XXX

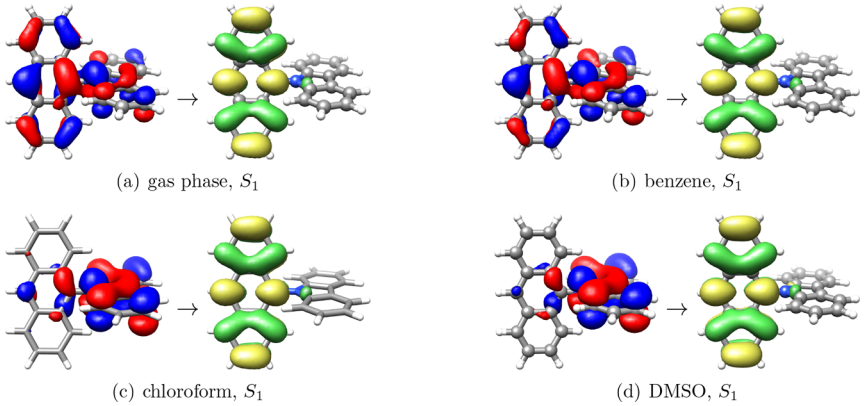


Figure 3. NTOs for C9A from ADC(2)/aug-cc-VTZ calculations at the ADC(2)/def2-TZVPP optimized S_1 geometries using in solution the PTED(LR) coupling scheme. For each environment, the occupied NTO is shown on the left side in blue and red and the virtual NTO on the right side in green and yellow.

solution, the CT contribution to S_1 and $\mu(S_1)$ decreases and the CT contribution to S_2 and $\mu(S_2)$ increases with increasing dielectric constant of the solvent. In polar solvents like acetonitrile and DMSO, S_1 is mostly a local HOMO−LUMO transition on the anthracene unit and S_2 is mostly a CT transition.

In the gas phase, the S_1 equilibrium structure has at the ADC(2)/def2-TZVPP level with $\tau = 59°$ a smaller twist angle than the ground-state structure, which allows a larger mixing between the LE and the CT configurations. The decrease of τ from 71° in S_0 to 59° in S_1 agrees well with the reduction of τ upon excitation to S_1 by 13.5° found in ref 57 for potential energy curves fitted to fluorescence excitation spectra. In line with the reduced twisting angle, S_1 has, at its equilibrium structure, a smaller CT contribution and a smaller dipole moment (3.8 D) than at the ground-state geometry.

In solution, when also the reaction field of the solvent is equilibrated with the charge distribution in the S_1 state, the torsion angle increases with increasing solvent polarity and reaches, in acetonitrile and DMSO with 73°, the same value as in the ground state. In contrast to what was found above for the vertical excitations in the S_0 equilibrium geometries, the CT contribution to S_1 increases in the excited-state equilibrium structure with solvent polarity. Already in chloroform (ϵ_r = 4.81), the S_1 state has at its equilibrium structure a predominantly CT character as seen from the NTOs in Figure 3. Accompanied by this change in the electronic structure of S_1, its dipole moment at the excited-state equilibrium geometry increases in solution strongly with the solvent polarity from 4.7 D in perfluoro-*n*-hexane to 13.9 D in DMSO (cf. Table 5).

With increasing solvent polarity and CT character of the excited state, the experimental fluorescence emission band maxima red-shift from 3.06 eV in perfluoro-*n*-hexane to 2.59 eV in DMSO. The decrease of $\tilde{\nu}_{max}^{em}$ is roughly proportional to the square of the solvent polarity/polarizability (SPP) parameter proposed in ref 59. The computed vertical deexcitation energies from S_1 reproduce this behavior with the SPP value (see Figure 4). Compared to the experimental values for $\tilde{\nu}_{max}^{em}$, the PTED(LR)-COSMO-ADC(2) results in the aug-cc-pVTZ basis are too low by 0.22 eV (in chloroform) to 0.38 eV (in acetonitrile), without a clear trend of the error with the SPP value. Exceptions are the results for benzene and 1,4-dioxane, which deviate only by, respectively, 0.12 and 0.09 eV from $\tilde{\nu}_{max}^{em}$. The dielectric constants of benzene and 1,4-dioxane are slightly smaller than for triethylamine (see Table 4), and the refractive

Table 5. Torsion Angle (τ), Vertical Deexcitation Energies ($\Delta E_\perp$), and Excited-State Dipole Moments ($\mu(S_1)$), Computed at the PTED(LR)-ADC(2)/aug-cc-pVTZ Level at the PTED(LR)-ADC(2)/def2-TZVPP Optimized S_1 Structures[a]

solvent	SPP[d]	τ (°)	$\Delta E_\perp$	$\tilde{\nu}_{max}^{em}$ [e]	T_e [f]	$\mu(S_1)$
vacuum	0.000	59	2.78 (3.06)		3.00	3.8
perfluorohexane	0.214	60	2.75 (3.04)	3.06	2.96	4.7
n-hexane	0.519	60	2.73 (3.03)	2.99	2.95	5.3
triethylamine	0.617	63	2.71 (3.03)	2.95	2.93	6.9
benzene	0.667	60	2.72 (3.03)	2.84	2.93	6.0
1,4-dioxane	0.701	61	2.72 (3.03)	2.81	2.94	6.1
chloroform	0.786	67	2.55 (2.91)	2.77	2.88	11.3
chlorobenzene	0.824	68	2.53 (2.89)	2.80	2.87	11.7
dichloromethane	0.876	70	2.42 (2.78)	2.72	2.84	12.7
acetonitrile	0.895	73	2.25 (2.61)	2.62	2.79	13.8
DMA[b]	0.970	73	2.27 (2.64)	2.67	2.79	13.8
DMSO[c]	1.000	73	2.27 (2.64)	2.59	2.78	13.9

[a]Extrapolated vertical CCSDR(3) excitation energies are given in parentheses; dipole moments are in Debye, and excitation energies and band maxima are in eV. [b]*N*,*N*-dimethylacetamide. [c]Dimethyl sulfoxide. [d]Solvent polarity/polarizability (SPP) parameter from ref 59. [e]Experimental fluorescence emission maxima from ref 59. [f]Adiabatic excitation energy relative to the ground-state minimum.

indices are similar (benzene: 1.50; 1,4-dioxane: 1.42; triethylamine: 1.40). Accordingly, the calculated vertical deexcitation energies in benzene and 1,4-dioxane are slightly higher than those in triethylamine. Nevertheless, their SPP values are higher and $\tilde{\nu}_{max}^{em}$ are lower than for triethylamine, which can only be caused by solute−solvent interactions that are not reflected in the macroscopic dielectric constant and the refractive index. The overall red-shift of the computed results compared to the experimental values originates most likely, as for the TICT state in DMABN to a certain extent, from the underestimation of CT transition energies by the second-order methods ADC(2) and CC2. To estimate the contribution from higher-order correlation effects on the vertical deexcitation energies, we determined the estimated PTED(LR)-CCSDR(3) results by adding to the PTED(LR)-ADC(2)/aug-cc-pVTZ values the difference between CCSDR(3)/def2-SVP and ADC(2)/def2-SVP excitation energies, both computed in the reaction field potential taken from a PTED(LR)-ADC(2)/def2-SVP calculation:

https://doi.org/10.1021/acs.jpca.5c02873
J. Phys. Chem. A XXXX, XXX, XXX−XXX

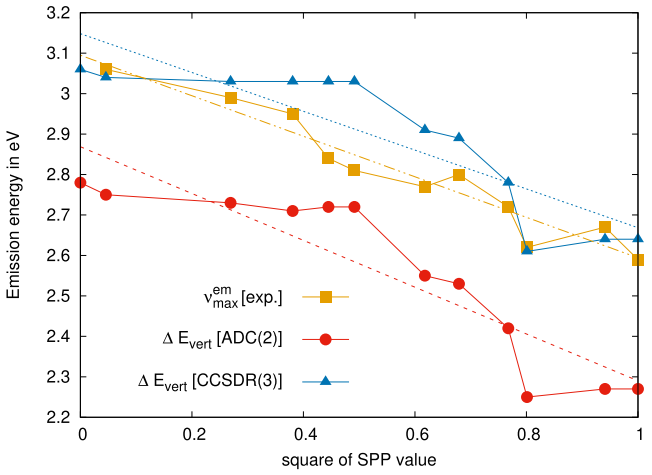


Figure 4. Experimental fluorescence band maxima and computed vertical deexcitation energies from S_1 in C9A plotted against the square of the SPP value.

$$E^{est}_{\text{PTED(LR)-CCSDR(3)}} = E_{\text{PTED(LR)-ADC(2)}} + [E_{\text{PTED}_{\text{ADC(2)}}\text{-CCSDR(3)}_{\text{RVS}}} - E_{\text{PTED}_{\text{ADC(2)}}\text{-ADC(2)}_{\text{RVS}}}] \quad (57)$$

For the calculation of the CCSDR(3) correction, we used again the RVS approximation and excluded the highest 151 virtual MOs, which correspond to a cutoff of ≈ 2 E_h. The results are listed in Table 5 in parentheses. The CCSDR(3) correction blue-shifts the computed excitation energies almost homogeneously by 0.28 eV. With the exception of the results for benzene, 1,4-dioxane, and chloroform, they agree with the experimental emission band maxima within 0.1 eV. The results for the outliers benzene and 1,4-dioxane lie also for the estimated PTED(LR)-CCSDR(3) results above the regression line for a linear fit versus the square of SPP. This supports the assumption that specific interactions that cannot be captured by a continuum solvation model are partially responsible for the remaining deviation from the experiment.

SUMMARY AND CONCLUSIONS

Excited states are often heavily affected by solvent effects, particularly those with bright transitions or transitions with a significant charge-transfer character. An accurate description of such effects in the context of SCRF theory is associated with many difficulties. Different contributions need to be accounted for, which are commonly differentiated into LR, important for bright transitions, and SS contributions, important for CT transitions. Furthermore, processes involving the relaxation of the excited-state geometry, such as fluorescence or phosphorescence, require us to compute analytic gradients for excited states. This becomes difficult if both states with CT and LE character are involved and need to be treated in a balanced way, as this requires a coupling scheme that includes both the LR and the SS contributions to the reaction field.

In this work, we derived for ADC(2) and CC2 the equations for analytic excited-state gradients for a state-specific PTED coupling scheme, which includes the LR contribution, originally proposed in ref 21 for COSMO-ADC(2) excitation energies. An implementation of the gradients for this coupling scheme, which we denote as PTED(LR) in the ricc2 program of TURBOMOLE and applications, is presented for the continuum solvation model COSMO and the atomistic PE approach. To the best of our knowledge, this is the first implementation of analytic excited-state gradients for a coupling scheme including both the LR and SS contributions and capable of treating bright LE and CT states in a balanced manner.

Using this implementation, we investigated the fluorescence in nonpolar and polar solutions for two chromophores, DMABN and C9A, both having low-lying excited states with a bright local excited and CT character. For DMABN, in particular, the geometry of the TICT state and its changes with solvent polarity were investigated. In contrast to the post-SCF coupling scheme, which includes only the LR contributions, the PTED(LR) scheme yields physically reasonable results. After including higher-order correlation effects via single-point CCSD and CC3 calculations, the computed deexcitation energies are for the LE and the TICT states in good agreement with experimental fluorescence band maxima for solvents covering a wide range of polarity. We further examined the effects of complexing the DMABN chromophore by curcubit[7]uril, showing, in particular, how the TICT state is affected by this additional environment. Finally, we investigated the solvent effects on the lowest two excited states of C9A, which have a delocalized nature with a mixed local excited and CT character. Here, the distribution of the LE and CT contributions between S_1 and S_2 is strongly coupled to the polarity of the solvent and the torsion angle between the carbazole and the anthryl groups. This leads to a roughly quadratic dependence of the Stokes shift on the SPP parameter, which could be reproduced with the PTED(LR) coupling scheme.

Compared to post-SCF and other coupling schemes that avoid including the state-specific relaxation of the reaction field in the presence of the final state's charge distribution in a self-consistent manner, the PTED(LR) scheme comes with computational costs that are about an order of magnitude higher and is limited to only a few of the lowest excited states. Nevertheless, due to its high accuracy and its property to provide a balanced description of bright local excited and CT excitations, we expect that PTED(LR), in particular in combination with ADC(2) and CC2, will become an increasingly important tool for the calculation of excited-state properties of molecules in solution.

ASSOCIATED CONTENT

Data Availability Statement

All structures, input files, and output files with the original data are available in a Zenodo data repository.[60]

AUTHOR INFORMATION

Corresponding Authors

Christof Hättig − *Lehrstuhl für Theoretische Chemie, Ruhr-Universität Bochum, 44801 Bochum, Germany;* orcid.org/0000-0002-5752-2710; Email: christof.haettig@rub.de

Ansgar Pausch − *Theoretical Chemistry, Vrije Universiteit Amsterdam, 1081HV Amsterdam, The Netherlands;* orcid.org/0000-0003-1895-2037; Email: a.i.pausch@vu.nl

Complete contact information is available at: https://pubs.acs.org/10.1021/acs.jpca.5c02873

Notes

The authors declare no competing financial interest.

https://doi.org/10.1021/acs.jpca.5c02873
J. Phys. Chem. A XXXX, XXX, XXX−XXX

■ ACKNOWLEDGMENTS

This article was funded by the Deutsche Forschungsgemeinschaft (DFG, German Research Foundation) under Germany's Excellence Strategy-EXC 2033-390677874-RESOLV. A.P. gratefully acknowledges support from the Walter Benjamin Programme funded through DFG-529675149.

■ REFERENCES

(1) Homocianu, M. Exploring solvatochromism: A comprehensive analysis of research data. *Microchemical Journal* **2024**, *198*, No. 110166.
(2) Senthilkumar, S.; Nath, S.; Pal, H. Photophysical Properties of Coumarin-30 Dye in Aprotic and Protic Solvents of Varying Polarities. *Photochem. Photobiol.* **2004**, *80*, 104−111.
(3) Rettig, W. Charge Separation in Excited States of Decoupled Systems—TICT Compounds and Implications Regarding the Development of New Laser Dyes and the Primary Process of Vision and Photosynthesis. *Angewandte Chemie International Edition in English* **1986**, *25*, 971−988.
(4) Catalán, J. On the dual emission of p-dimethylaminobenzonitrile and its photophysical implications. *Phys. Chem. Chem. Phys.* **2013**, *15*, 8811−8820.
(5) Jacquemin, D.; Chibani, S.; Le Guennic, B.; Mennucci, B. Solvent Effects on Cyanine Derivatives: A PCM Investigation. *J. Phys. Chem. A* **2014**, *118*, 5343−5348.
(6) von Arnim, M.; Ahlrichs, R. Geometry optimization in generalized natural internal coordinates. *J. Chem. Phys.* **1999**, *111*, 9183−9190.
(7) Constanciel, R.; Contreras, R. Self consistent field theory of solvent effects representation by continuum models: Introduction of desolvation contribution. *Theor. Chim. Acta* **1984**, *65*, 1−11.
(8) Olsen, J.; Jørgensen, P. Linear and nonlinear response functions for an exact state and for an MCSCF state. *J. Chem. Phys.* **1985**, *82*, 3235−3264.
(9) Christiansen, O.; Jørgensen, P.; Hättig, C. Response functions from Fourier component variational perturbation theory applied to a time-averaged quasienergy. *Int. J. Quantum Chem.* **1998**, *68*, 1−52.
(10) Klamt, A.; Schüürmann, G. COSMO: a new approach to dielectric screening in solvents with explicit expressions for the screening energy and its gradient. *J. Chem. Soc., Perkin Trans.* **1993**, *2*, 799−805.
(11) Diedenhofen, M.; Klamt, A. COSMO-RS as a tool for property prediction of IL mixtures—A review. *Fluid Phase Equilib.* **2010**, *294*, 31−38.
(12) Guido, C. A.; Scalmani, G.; Mennucci, B.; Jacquemin, D. Excited state gradients for a state-specific continuum solvation approach: The vertical excitation model within a Lagrangian TDDFT formulation. *J. Chem. Phys.* **2017**, *146*, 204106.
(13) Miertuš, S.; Scrocco, E.; Tomasi, J. Electrostatic interaction of a solute with a continuum. A direct utilizaion of AB initio molecular potentials for the prevision of solvent effects. *Chem. Phys.* **1981**, *55*, 117−129.
(14) Cammi, R.; Fukuda, R.; Ehara, M.; Nakatsuji, H. Symmetry-adapted cluster and symmetry-adapted cluster-configuration interaction method in the polarizable continuum model: Theory of the solvent effect on the electronic excitation of molecules in solution. *J. Chem. Phys.* **2010**, *133*, No. 024104.
(15) Cammi, R. Coupled-cluster theories for the polarizable continuum model. II. Analytical gradients for excited states of molecular solutes by the equation of motion coupled-cluster method. *Int. J. Quantum Chem.* **2010**, *110*, 3040−3052.
(16) Caricato, M. Absorption and Emission Spectra of Solvated Molecules with the EOM−CCSD−PCM Method. *J. Chem. Theory Comput.* **2012**, *8*, 4494−4502.
(17) Caricato, M. CCSD-PCM Excited State Energy Gradients with the Linear Response Singles Approximation to Study the Photochemistry of Molecules in Solution. *ChemPhotoChem.* **2019**, *3*, 747−754.
(18) Khani, S. K.; Khah, A. M.; Hättig, C. COSMO-RI-ADC(2) excitation energies and excited state gradients. *Phys. Chem. Chem. Phys.* **2018**, *20*, 16354−16363.
(19) Marefat Khah, A.; Karbalaei Khani, S.; Hättig, C. Analytic Excited State Gradients for the QM/MM Polarizable Embedded Second-Order Algebraic Diagrammatic Construction for the Polarization Propagator PE-ADC(2). *J. Chem. Theory Comput.* **2018**, *14*, 4640−4650.
(20) Christiansen, O.; Koch, H.; Jørgensen, P. The second-order approximate coupled cluster singles and doubles model CC2. *Chem. Phys. Lett.* **1995**, *243*, 409−418.
(21) Lunkenheimer, B.; Köhn, A. Solvent Effects on Electronically Excited States Using the Conductor-Like Screening Model and the Second-Order Correlated Method ADC(2). *J. Chem. Theory Comput.* **2013**, *9*, 977−994.
(22) Olsen, J. M.; Aidas, K.; Kongsted, J. Excited States in Solution through Polarizable Embedding. *J. Chem. Theory Comput.* **2010**, *6*, 3721−3734.
(23) York, D. M.; Karplus, M. A Smooth Solvation Potential Based on the Conductor-Like Screening Model. *J. Phys. Chem. A* **1999**, *103*, 11060−11079.
(24) Garcia-Ratés, M.; Neese, F. Effect of the Solute Cavity on the Solvation Energy and its Derivatives within the Framework of the Gaussian Charge Scheme. *J. Comput. Chem.* **2020**, *41*, 922−939.
(25) Pausch, A. Consistent Analytical Second Derivatives of the Kohn−Sham DFT Energy in the Framework of the Conductor-Like Screening Model through Gaussian Charge Distributions. *J. Chem. Theory Comput.* **2024**, *20*, 3169−3183.
(26) Helgaker, T.; Jørgensen, P.; Olsen, J. *Molecular Electronic-Structure Theory*; John Wiley & Sons: New York, 2000.
(27) Sneskov, K.; Schwabe, T.; Kongsted, J.; Christiansen, O. The polarizable embedding coupled cluster method. *J. Chem. Phys.* **2011**, *134*, 104108.
(28) Schwabe, T.; Sneskov, K.; Olsen, J. M. H.; Kongsted, J.; Christiansen, O.; Hättig, C. PERI-CC2: A Polarizable Embeddded RI-CC2Method. *J. Chem. Theory Comput.* **2012**, *8*, 3274−3283.
(29) Marefat Khah, A.; Reinholdt, P.; Olsen, J. M. H.; Kongsted, J.; Hättig, C. Avoiding Electron Spill-Out in QM/MM Calculations on Excited States with Simple Pseudopotentials. *J. Chem. Theory Comput.* **2020**, *16*, 1373−1381.
(30) Hättig, C. Geometry optimizations with the coupled-cluster model CC2 using the resolution-of-the-identity approximation. *J. Chem. Phys.* **2003**, *118*, 7751−7761.
(31) Köhn, A.; Hättig, C. Analytic gradients for excited states in the coupled-cluster model CC2 employing the resolution-of-the-identity approximation. *J. Chem. Phys.* **2003**, *119*, 5021−5036.
(32) Tew, D. P.; Hättig, C.; Graf, N. K. Anharmonic excited state frequencies of para-difluorobenzene, toluene and catechol using analytic RI-CC2 second derivatives. *Phys. Chem. Chem. Phys.* **2019**, *21*, 14063−14072.
(33) Schirmer, J. Beyond the random phase approximation: A new approximation scheme for the polarization propagator. *Phys. Rev. A* **1982**, *26*, 2395−2416.
(34) Trofimov, A. B.; Schirmer, J. An efficient polarization propagator approach to valence electron-excitation spectra. *J. Phys. B* **1995**, *28*, 2299−2324.
(35) Hättig, C. Structure optimizations for excited states with correlated second-order methods: CC2, CIS(D∞), and ADC(2). *Adv. Quantum Chem.* **2005**, *50*, 37−60.
(36) del Valle, F.; Tomasi, J. Electron correlation and solvation effects. I. Basic formulation and preliminary attempt to include the electron correlation in the quantum mechanical polarizable continuum model so as to study solvation phenomena. *Chem. Phys.* **1991**, *150*, 139−150.
(37) Cammi, R. *Continuum Solvation Models in Chemical Physics: From Theory to Applications*; Mennucci, B.; Cammi, R., Eds.; John Wiley & Sons, 2007; Chapter 1.5.
(38) Cammi, R. Quantum cluster theory for the polarizable continuum model. I. The CCSD level with analytical first and second derivatives. *J. Chem. Phys.* **2009**, *131*, 164104.

https://doi.org/10.1021/acs.jpca.5c02873
J. Phys. Chem. A XXXX, XXX, XXX−XXX

(39) Cammi, R. Coupled-cluster theory for the polarizable continuum model. III. A response theory for molecules in solution. *Int. J. Quantum Chem.* **2012**, *112*, 2547−2560.
(40) Cammi, R.; Corni, S.; Mennucci, B.; Tomasi, J. Electronic excitation energies of molecules in solution: State specific and linear response methods for nonequilibrium continuum solvation models. *J. Chem. Phys.* **2005**, *122*, 104513.
(41) Corni, S.; Cammi, R.; Mennucci, B.; Tomasi, J. Electronic excitation energies of molecules in solution within continuum solvation models: Investigating the discrepancy between state-specific and linear-response methods. *J. Chem. Phys.* **2005**, *123*, 134512.
(42) Hättig, C.; Weigend, F. CC2 excitation energy calculations on large molecules using the resolution of the identity approximation. *J. Chem. Phys.* **2000**, *113*, 5154−5161.
(43) *Developers' version of TURBOMOLE V7.8 2023, a development of University of Karlsruhe and Forschungszentrum Karlsruhe GmbH, 1989−2007, TURBOMOLE GmbH*, since 2007; available from https://www.turbomole.org (retrieved April 4, 2024).
(44) Franzke, Y. J.; Holzer, C.; Andersen, J. H.; Begušić, T.; Bruder, F.; Coriani, S.; Della Sala, F.; Fabiano, E.; Fedotov, D. A.; Fürst, S.; et al. TURBOMOLE: Today and Tomorrow. *J. Chem. Theory Comput.* **2023**, *19*, 6859−6890.
(45) Gómez, S.; Soysal, E. N.; Worth, G. A. Micro-Solvated DMABN: Excited State Quantum Dynamics and Dual Fluorescence Spectra. *Molecules* **2021**, *26*, 7247.
(46) Georgieva, I.; Aquino, A. J. A.; Plasser, F.; Trendafilova, N.; Köhn, A.; Lischka, H. Intramolecular Charge-Transfer Excited-State Processes in 4-(N,N-Dimethylamino)benzonitrile: The Role of Twisting and the $\pi\sigma^*$ State. *J. Phys. Chem. A* **2015**, *119*, 6232−6243.
(47) Köhn, A.; Hättig, C. On the Nature of the Low-Lying Singlet States of 4-(Dimethyl-amino)benzonitrile. *J. Am. Chem. Soc.* **2004**, *126*, 7399−7410.
(48) Rappoport, D.; Furche, F. Photoinduced Intramolecular Charge Transfer in 4-(Dimethyl)aminobenzonitrile−A Theoretical Perspective. *J. Am. Chem. Soc.* **2004**, *126*, 1277−1284.
(49) Yoshihara, T.; Galievsky, V. A.; Druzhinin, S. I.; Saha, S.; Zachariasse, K. A. Singlet excited state dipole moments of dual fluorescent N-phenylpyrroles and 4-(dimethylamino)benzonitrile from solvatochromic and thermochromic spectral shifts. *Photochemical & Photobiological Sciences* **2003**, *2*, 342−353.
(50) Marquez, C.; Nau, W. M. Polarizabilities Inside Molecular Containers. *Angew. Chem., Int. Ed.* **2001**, *40*, 4387−4390.
(51) Dunning, T. H. Gaussian basis sets for use in correlated molecular calculations. I. The atoms boron through neon and hydrogen. *J. Chem. Phys.* **1989**, *90*, 1007−1023.
(52) Weigend, F.; Köhn, A.; Hättig, C. Efficient use of the correlation consistent basis sets in resolution of the identity MP2 calculations. *J. Chem. Phys.* **2002**, *116*, 3175−3183.
(53) Weigend, F.; Ahlrichs, R. Balanced basis sets of split valence, triple zeta valence and quadruple zeta valence quality for H to Rn: Design and assessment of accuracy. *Phys. Chem. Chem. Phys.* **2005**, *7*, 3297.
(54) Weigend, F.; Häser, M.; Patzelt, H.; Ahlrichs, R. RI-MP2: optimized auxiliary basis sets and demonstration of efficiency. *Chem. Phys. Lett.* **1998**, *294*, 143−152.
(55) Kendall, R. A.; Dunning, T. H.; Harrison, R. J. Electron affinities of the first-row atoms revisited. Systematic basis sets and wave functions. *J. Chem. Phys.* **1992**, *96*, 6796−6806.
(56) Sayed, M.; Biedermann, F.; Uzunova, V. D.; Assaf, K. I.; Bhasikuttan, A. C.; Pal, H.; Nau, W. M.; Mohanty, J. Triple Emission from p-Dimethylaminobenzonitrile−Cucurbit[8]uril Triggers the Elusive Excimer Emission. *Chemistry−A. European Journal* **2015**, *21*, 691−696.
(57) Monte, C.; Roggan, A.; Subaric-Leitis, A.; Rettig, W.; Zimmermann, P. Resonance effects of diabatic surface crossing within the torsional spectrum of 9-(N-carbazolyl) anthracene observed by supersonic jet fluorescence spectroscopy. *J. Chem. Phys.* **1993**, *98*, 2580−2592.
(58) Evers, F.; Giraud-Girard, J.; Grimme, S.; Manz, J.; Monte, C.; Oppel, M.; Rettig, W.; Saalfrank, P.; Zimmermann, P. Absorption and Fluorescence Excitation Spectra of 9-(N-carbazolyl)-anthracene: Effects of Intramolecular Vibrational Redistribution and Diabatic Transitions Involving Electron Transfer. *J. Phys. Chem. A* **2001**, *105*, 2911−2924.
(59) Catalán, J.; Díaz, C.; López, V.; Pérez, P.; Claramunt, R. M. The TICT Mechanism in 9,9'-Biaryl Compounds: Solvatochromism of 9,9'-Bianthryl, N-(9-Anthryl)carbazole, and NN'-Bicarbazyl. *J. Phys. Chem.* **1996**, *100*, 18392−18398.
(60) Hättig, C.; Pausch, A. Raw data for: "Gradients of ground and excited states for CC2 and ADC(2) in polarizable continuum and atomistic embeddings within a generalized PTED coupling scheme". 2025; DOI: 10.5281/zenodo.15254097, Data Set published on Zenodo; accessed: April 21, 2025.

https://doi.org/10.1021/acs.jpca.5c02873
J. Phys. Chem. A XXXX, XXX, XXX−XXX